

TYCHO-GAIA ASTROMETRIC SOLUTION PARALLAXES AND PROPER MOTIONS FOR 5 GALACTIC GLOBULAR CLUSTERS

LAURA L. WATKINS AND ROELAND P. VAN DER MAREL
Space Telescope Science Institute, 3700 San Martin Drive, Baltimore MD 21218, USA
ApJ draft, 13 February 2022

ABSTRACT

We perform a systematic search for Galactic globular cluster (GC) stars in the Tycho-*Gaia* Astrometric Solution (TGAS) catalogue that formed part of *Gaia* Data Release 1 (DR1), and identify 5 members of NGC 104 (47 Tucanae), 1 member of NGC 5272 (M3), 5 members of NGC 6121 (M4), 7 members of NGC 6397, and 2 members of NGC 6656 (M22). By taking a weighted average of the member stars, fully accounting for the correlations between parameter estimates, we estimate the parallax (and, hence, distance) and proper motion (PM) of the GCs. This provides a homogeneous PM study of multiple GCs based on an astrometric catalogue with small and well-controlled systematic errors, and yields random PM errors that are similar to existing measurements. Detailed comparison to the available *Hubble Space Telescope* (*HST*) measurements generally shows excellent agreement, validating the astrometric quality of both TGAS and *HST*. By contrast, comparison to ground-based measurements shows that some of those must have systematic errors exceeding the random errors. Our parallax estimates have uncertainties an order of magnitude larger than previous studies, but nevertheless imply distances consistent with previous estimates. By combining our PM measurements with literature positions, distances and radial velocities, we measure Galactocentric space motions for the clusters and find that these are also in good agreement with previous orbital analyses. Our results highlight the future promise of *Gaia* for the determining accurate distances and PMs of Galactic GCs, which will provide crucial constraints on the near end of the cosmic distance ladder, and provide accurate GC orbital histories.

Keywords: globular clusters: individual (NGC 104 (47 Tucanae), NGC 5272 (M3), NGC 6121 (M4), NGC 6397, NGC 6656 (M22)) – parallaxes – proper motions – stars: kinematics and dynamics

1. INTRODUCTION

Accurate distances and space motions of Galactic globular clusters are difficult but incredibly valuable to measure: improved constraints will have implications for the origin and evolution of the clusters themselves, for the structure of the Milky Way, and for the fine-tuning of cosmological models.

Prevailing theory for the origin of the MW’s GC population is that some GCs were formed outside of the MW and later accreted while the rest were formed in situ (eg. Mackey & Gilmore 2004). The different origins and histories for the accreted and in-situ populations will manifest in their orbits (eg. Zhu et al. 2016) and imprint on their internal dynamics (eg. Webb et al. 2014; Zocchi et al. 2016), so determining which GCs belong to which population and analysing the differences between them will advance our understanding of cluster formation and evolution.

Moreover, accurate 6-dimensional phase space information for the GCs will allow us to constrain cluster orbits (eg. Küpper et al. 2015), which will indicate which clusters have been most affected by tides, and if any known GCs could be the missing progenitors of tidal streams whose origin is unknown. Cluster orbits will also be beneficial in constraining the inner shape of the Galactic halo (eg. Pearson et al. 2015).

Local GCs populate the short end of the cosmological distance ladder, so improved distances will provide important cosmology-independent verification for cosmological models (Verde et al. 2013). Distances are also a key ingredient in GC age determination using the luminosity of the main-sequence turn off (e.g. Chaboyer 1995) and currently the distance uncertainties in such analyses dominate over other sources of error. Accurate GC ages are of special interest as GCs are

among the oldest objects in the Universe for which ages are known and so help to constrain the age of the Universe (eg. Krauss & Chaboyer 2003).

Not only are distances and PMs useful measurements to have, but multiple measurements, using different data types and analysis methods, improve accuracy and ensure that the measurements not biased. GC distances are typically estimated photometrically using “standard candles”, such as RR Lyraes or the position of the horizontal branch. However, it is also possible to estimate distances from kinematic data by comparing line-of-sight velocity and PMs measurements. In Watkins et al. (2015a), we estimated dynamical distances for 15 Galactic GCs using the *Hubble Space Telescope* (*HST*) Proper Motion (HSTPROMO)¹ GC catalogues (Bellini et al. 2014) and compared them to the photometric distance estimates compiled in Harris (1996, 2010 edition, hereafter H96). Overall we showed that the two very different methods of distance estimation agreed very well, implying that both methods are robust and unbiased, however a further comparison against parallax distances will provide an useful additional test.

Absolute PMs have previously been measured from the ground for 63 Galactic GCs (Dinescu et al. 1997, 1999b,a, 2003; Casetti-Dinescu et al. 2007, 2010, 2013, hereafter CD13)² as part of the Southern Proper Motion (SPM) Program. These measurements are heterogeneous as the method used to correct the PMs to an inertial reference frame varied from cluster to cluster. Also, in some cases, the measurements represent a combination of multiple determinations (by including other PM determinations from other ground- and space-based sources) and not a single determination. Never-

¹ <http://www.stsci.edu/~marel/hstpromo.html>

² A compilation is available at <http://www.astro.yale.edu/dana/gc.html>.

theless, independent PM measurements for these GCs will be incredibly helpful to verify their accuracy and to assess the consistency of the different methods.

Gaia will provide five-parameter astrometric solutions – positions, parallaxes and PMs – for objects brighter than ~ 20 mag and so will be tremendously useful for analysing both internal and global PMs for Galactic GCs, and their distances³. Proper motion and parallax are degenerate, and a sufficiently long baseline is needed to disentangle the two; at the time of the first *Gaia* data release (DR1, September 2016, [Gaia Collaboration et al. 2016](#)), parallaxes and PMs were not measurable with *Gaia* data alone. The first *Gaia*-only PM measurements are projected for release in late 2017, and the final (and most accurate) PMs will be released only in 2022. However, by crossmatching the *Gaia* catalogue with the *Hipparcos* Tycho2 catalogue ([Høg et al. 2000](#)), it is possible to measure PMs (and parallaxes) for stars in both datasets: the Tycho-*Gaia* Astrometric Solution (TGAS, [Michalik et al. 2015](#); [Lindegren et al. 2016](#)). Combining Tycho2 and *Gaia* data together offers an extended baseline for PM studies that has made PM analyses achievable for a few million stars with the *Gaia* DR1. Although not ideally suited to dynamical studies of objects within the Local Group, TGAS has already been used to measure the rotation fields of the Magellanic Clouds ([van der Marel & Sahlmann 2016](#)). Here, we search for Galactic GC stars in the TGAS catalogue.

We outline our cluster-member determination in [Section 2](#), present our parallax and PM results in [Section 3](#), discuss the implied space motions and orbits of the clusters in [Section 4](#), and conclude in [Section 5](#).

2. CLUSTER MEMBERSHIP DETERMINATION

To determine likely GC members, we wish to search for stars that are close to a GC centre on the plane of sky and then check for consistency with previous PM and parallax estimates, and typical GC isochrones. We also wish to consider predictions for the PMs, parallaxes and photometry expected for MW stars along the line-of-sight to the GC to rule out contaminants.

2.1. Proximity

To estimate how many Galactic GC stars may exist in the TGAS catalogue, we wish to count the number of stars found within some limiting radius from the centre of each GC on the plane of the sky. We begin with the [H96](#) Galactic GC catalogue from which we extract cluster centre coordinates, concentrations, and core radii. Although the catalogue contains data for 157 Galactic GCs, we were only able to proceed with 156 GCs as Pyxis has no concentration or core radius estimate listed.⁴

We use the concentrations c and core radii R_{core} to estimate the tidal radii R_{tidal} of the GCs via,

$$R_{\text{tidal}} = 10^c R_{\text{core}}. \quad (1)$$

This is not generally considered to be a robust method of tidal-radius determination and is likely to underestimate the true extent of a GC. These tidal radii estimates assume an underlying

³ Note that [Astraatmadja & Bailer-Jones \(2016\)](#) caution that estimation of distances from *Gaia* parallaxes is not as simple as inverting the parallaxes as the parallax uncertainties are non-negligible, and must be done using rigorous statistical analysis.

⁴ This does not affect our analysis as Pyxis is too distant to have stars with sufficient apparent brightness in the Tycho2 catalogue.

King profile, however GCs are generally better fit by Wilson models (eg. [McLaughlin & van der Marel 2005](#)), which are still finite in extent but are more extended than King models. Furthermore, a GC that is tidally disrupting may have member stars outside of its formal tidal radius. However this method is sufficient for our purposes, which is simply to estimate the approximate extent of the clusters on the plane of the sky. To mitigate the possibility of underestimating the true extent of the cluster, we adopt $2R_{\text{tidal}}$ as the limiting radius within which to search for GC members.

Then, for each GC in turn, we extracted from the TGAS catalogue all stars within $2R_{\text{tidal}}$ of the cluster centre. We did this for all 156 GCs with no cuts on heliocentric distance, magnitude, or central velocity dispersion (all of which could affect the likelihood that a star close to the centre in projection is a true cluster member). In total, we identified 4268 stars within $2R_{\text{tidal}}$ of the centre of a GC across 142 clusters.

2.2. Distance and Extinction

Some of these clusters are relatively far away, and others are in regions of high extinction, so it is likely that true GC members will be rendered too faint for detection with TGAS. So we wish to determine the expected apparent magnitude of the brightest star in any given GC, and then the number of observed stars fainter than this limit.

To do this, we select for each star the V_T magnitude from the Tycho2 catalogue or the V magnitude from the *Hipparcos* catalogue, depending on the original catalogue of origin. Both *Hipparcos* V and Tycho2 V_T are very similar and correspond to the *HST* F555W filter, for which we have isochrones and extinction coefficients. We then take a typical GC isochrone from the Dartmouth Stellar Evolution Database ([Dotter et al. 2008](#)) with metallicity $[\text{Fe}/\text{H}] = -1.5$ dex, alpha-element abundance $[\alpha/\text{Fe}] = 0.2$ dex, and age $A = 11$ Gyr, and estimate the brightest magnitude the isochrone reaches.

For each cluster, we adjust the tip magnitude of the isochrone for GC distance and extinction along the line of sight using distance moduli calculated using distances from [H96](#), extinctions also from [H96](#), and extinction coefficients from [Sirianni et al. \(2005\)](#). To allow for magnitude uncertainties, we set the limiting magnitude at 0.5 mag brighter than the distance- and extinction-corrected tip of the isochrone, and count the number of stars fainter than this limiting magnitude. We will perform a more careful photometry check on our GC member candidates in [Section 2.5](#), this rather crude preliminary cut is intended to remove distant and highly-extincted clusters from further consideration. After these cuts, we are left with 967 stars across 30 clusters; the most distant lies at 10.3 kpc. Cluster properties for these 30 clusters are given in [Table 1](#).

2.3. Parallax and Proper Motion

To determine which of these stars are likely to be cluster members, we wish to identify which stars have parallax and PM measurements that are consistent with previous measurements for their nearby cluster.

TGAS provides parallaxes ϖ , and PMs ($\mu_{\alpha^*}, \mu_{\delta}$) for each star, along with uncertainties for each and correlation coefficients among the parameters, from which we can construct a full 3-dimensional covariance matrix.

For the GCs, we adopt distances from [H96](#), which we then invert to determine parallax estimates. The [H96](#) distances have no formal error bars, so we adopt errors of 10% on our

Table 1
 Cluster properties.

Cluster	α	δ	c	R_{core}	R_{tidal}	D	μ_{α^*}	μ_{δ}	$E(B-V)$	[Fe/H]	v_r	σ_v
(1)	(deg)	(deg)	(4)	(arcmin)	(arcmin)	(kpc)	(mas/yr)	(mas/yr)	(10)	(dex)	(km/s)	(km/s)
NGC 104	6.02	-72.08	2.07	0.360	42.296	4.5	5.63 ± 0.21	-2.73 ± 0.29	0.04	-0.72	-18.0 ± 0.1	11.0 ± 0.3
NGC 288	13.19	-26.58	0.99	1.350	13.193	8.9	4.67 ± 0.22	-5.60 ± 0.35	0.03	-1.32	-45.4 ± 0.2	2.9 ± 0.3
NGC 3201	154.40	-46.41	1.29	1.300	25.348	4.9	5.28 ± 0.32	-0.98 ± 0.33	0.24	-1.59	494.0 ± 0.2	5.0 ± 0.2
NGC 4372	186.44	-72.66	1.30	1.750	34.917	5.8	-6.49 ± 0.33	3.71 ± 0.32	0.39	-2.17	72.3 ± 1.2	...
NGC 4590	189.87	-26.74	1.41	0.580	14.908	10.3	-3.76 ± 0.66	1.79 ± 0.62	0.05	-2.23	-94.7 ± 0.2	2.5 ± 0.4
NGC 4833	194.89	-70.88	1.25	1.000	17.783	6.6	-8.11 ± 0.35	-0.96 ± 0.34	0.32	-1.85	200.2 ± 1.2	...
NGC 5139	201.70	-47.48	1.31	2.370	48.389	5.2	-5.08 ± 0.35	-3.57 ± 0.34	0.12	-1.53	232.1 ± 0.1	16.8 ± 0.3
NGC 5272	205.55	28.38	1.89	0.370	28.721	10.2	-0.12 ± 0.61	-2.67 ± 0.40	0.01	-1.50	-147.6 ± 0.2	5.5 ± 0.3
NGC 5904	229.64	2.08	1.73	0.440	23.629	7.5	4.27 ± 0.60	-11.30 ± 1.46	0.03	-1.29	53.2 ± 0.4	5.5 ± 0.4
NGC 5927	232.00	-50.67	1.60	0.420	16.721	7.7	-5.72 ± 0.39	-2.61 ± 0.40	0.45	-0.49	-107.5 ± 0.9	...
NGC 6121	245.90	-26.53	1.65	1.160	51.815	2.2	-12.66 ± 0.28	-19.39 ± 0.29	0.35	-1.16	70.7 ± 0.2	4.0 ± 0.2
NGC 6171	248.13	-13.05	1.53	0.560	18.975	6.4	-0.70 ± 0.90	-3.10 ± 1.00	0.33	-1.02	-34.1 ± 0.3	4.1 ± 0.3
NGC 6205	250.42	36.46	1.53	0.620	21.008	7.1	-0.10 ± 0.80	4.69 ± 0.81	0.02	-1.53	-244.2 ± 0.2	7.1 ± 0.4
NGC 6218	251.81	-1.95	1.34	0.790	17.283	4.8	1.15 ± 1.95	-7.75 ± 1.67	0.19	-1.37	-41.4 ± 0.2	4.5 ± 0.4
NGC 6254	254.29	-4.10	1.38	0.770	18.471	4.4	-5.75 ± 0.78	-4.75 ± 1.45	0.28	-1.56	75.2 ± 0.7	6.6 ± 0.8
NGC 6304	258.63	-29.46	1.80	0.210	13.250	5.9	-2.59 ± 0.29	-1.56 ± 0.29	0.54	-0.45	-107.3 ± 3.6	...
NGC 6341	259.28	43.14	1.68	0.260	12.444	8.3	-3.58 ± 0.89	-0.60 ± 0.60	0.02	-2.31	-120.0 ± 0.1	6.0 ± 0.4
NGC 6352	261.37	-48.42	1.10	0.830	10.449	5.6	0.22	-0.64	-137.0 ± 1.1	...
NGC 6362	262.98	-67.05	1.09	1.130	13.902	7.6	-3.09 ± 0.46	-3.83 ± 0.46	0.09	-0.99	-13.1 ± 0.6	2.8 ± 0.4
NGC 6397	265.18	-53.67	2.50	0.050	15.811	2.3	3.69 ± 0.29	-14.88 ± 0.26	0.18	-2.02	18.8 ± 0.1	4.5 ± 0.2
NGC 6541	272.01	-43.71	1.86	0.180	13.040	7.5	0.14	-1.81	-158.7 ± 2.3	8.2 ± 2.1
NGC 6624	275.92	-30.36	2.50	0.060	18.974	7.9	0.28	-0.44	53.9 ± 0.6	5.4 ± 0.5
NGC 6656	279.10	-23.90	1.38	1.330	31.904	3.2	7.37 ± 0.50	-3.95 ± 0.42	0.34	-1.70	-146.3 ± 0.2	7.8 ± 0.3
NGC 6681	280.80	-32.29	2.50	0.030	9.487	9.0	0.07	-1.62	220.3 ± 0.9	5.2 ± 0.5
NGC 6723	284.89	-36.63	1.11	0.830	10.692	8.7	-0.17 ± 0.45	-2.16 ± 0.50	0.05	-1.10	-94.5 ± 3.6	...
NGC 6752	287.72	-59.98	2.50	0.170	53.759	4.0	-0.69 ± 0.42	-2.85 ± 0.45	0.04	-1.54	-26.7 ± 0.2	4.9 ± 0.4
NGC 6779	289.15	30.18	1.38	0.440	10.555	9.4	0.30 ± 1.00	1.40 ± 1.00	0.26	-1.98	-135.6 ± 0.9	4.0 ± 0.6
NGC 6809	295.00	-30.96	0.93	1.800	15.320	5.4	-3.31 ± 0.94	-9.70 ± 0.55	0.08	-1.94	174.7 ± 0.3	4.0 ± 0.3
NGC 6838	298.44	18.78	1.15	0.630	8.899	4.0	-2.30 ± 0.80	-5.10 ± 0.80	0.25	-0.78	-22.8 ± 0.2	2.3 ± 0.2
NGC 7099	325.09	-23.18	2.50	0.060	18.974	8.1	1.42 ± 0.69	-7.71 ± 0.65	0.03	-2.27	-184.2 ± 0.2	5.5 ± 0.4

Notes. Columns: (1) cluster name; (2) Right Ascension; (3) Declination; (4) concentration; (5) core radius; (6) tidal radius; (7) heliocentric distance; (8) PM in Right Ascension; (9) PM in Declination; (10) extinction correction; (11) [Fe/H] metallicity; (12) heliocentric radial velocity; (13) central velocity dispersion. All values taken from H96, except PMs (columns 8 and 9), which were taken from CD13.

parallax estimates. For PM measurements, we use the CD13 catalogue. Only 26 of the 30 clusters with GC member candidates have PM measurements in this catalogue and so only these 26 GCs can be evaluated here.

For each cluster, we calculate the probability for the nearby stars of being a cluster member. For a star i with parallax and PM measurements \mathbf{m}_i and covariance \mathbf{C}_i , we ask what is the likelihood $\mathcal{L}_{\text{GC},i}$ that this star is a member of a GC with measurements \mathbf{m}_{GC} and covariance \mathbf{C}_{GC} ,

$$\begin{aligned} \mathcal{L}_{\text{GC},i} &= p(\mathbf{m}_i | \mathbf{C}_i, \mathbf{m}_{\text{GC}}, \mathbf{C}_{\text{GC}}) \\ &= \frac{\exp\left[-\frac{1}{2}(\mathbf{m}_i - \mathbf{m}_{\text{GC}})^T (\mathbf{C}_i + \mathbf{C}_{\text{GC}})^{-1} (\mathbf{m}_i - \mathbf{m}_{\text{GC}})\right]}{\sqrt{(2\pi)^3 |\mathbf{C}_i + \mathbf{C}_{\text{GC}}|}}, \end{aligned} \quad (2)$$

which is a standard 3-dimensional Gaussian. To construct the GC covariance matrix \mathbf{C}_{GC} , we assume that the errors are uncorrelated, so the diagonal terms are the squared uncertainties on the parallax and PM measurements and the off-diagonal elements are zero. We further add the GC velocity dispersion (H96) in quadrature to the PM terms to account for the expected spread in velocities.

This likelihood calculation assumes that all stars select near the cluster are equally likely to be members, but this is not the case. Stars close to the cluster centre of the cluster are more likely to be members than stars near to the $2R_{\text{tidal}}$ boundary, so we also calculate the likelihood of a star i with coordinates

(α_i, δ_i) being a member of the GC with centre $(\alpha_{GC}, \delta_{GC})$ as,

$$\begin{aligned} \mathcal{L}_{\alpha\delta,i} &= p(\alpha_i, \delta_i | \alpha_{GC}, \delta_{GC}, \sigma) \\ &= \exp \left[-\frac{1}{2\sigma^2} \left((\alpha_i - \alpha_{GC})^2 + (\delta_i - \delta_{GC})^2 \right) \right]. \end{aligned} \quad (3)$$

where we use $\sigma = \frac{1}{2}R_{\text{tidal}}$ to account for the approximate extent of the cluster. The uncertainties on the cluster centre coordinates and on the positions of the stars are negligible compared to the extent of the cluster, so we neglect the measurement errors in this calculation.

GC projected number density profiles are, of course, highly non-Gaussian, however the profiles in the outer regions of GCs are largely uncertain due to effect of tides and the scarcity of data there. This Gaussian weighting suffices to down-weight stars found further away from the cluster centre. Also note, that although we have used unnormalised Gaussians here as we are mostly concerned with how many tidal radii the star is away from the cluster centre, rather than the tidal radius itself. That is, a star $1R_{\text{tidal}}$ from the cluster centre should have the same $\mathcal{L}_{\alpha\delta,i}$ in all clusters, regardless of the value of R_{tidal} .

Finally, we can calculate the total likelihood that the star is a member of the cluster $\mathcal{L}_i = \mathcal{L}_{\text{PM},i} \times \mathcal{L}_{\alpha\delta,i}$. We keep all stars with $\mathcal{L}_i > -11$ as possible cluster members.⁵ This selects 64 stars across 15 clusters. All of the identified candidates are Tycho2 stars, no Hipparcos stars remain in our sample.

2.4. Radial Velocities

As a further test for membership, we wish to check whether the candidate cluster members have radial velocities (RVs) consistent with cluster membership. We cross-match our stars with the RAdial Velocity Experiment (RAVE, Kunder et al. 2016) catalogue to extract RVs, and find 15 stars in common between our high-likelihood sample and RAVE. Using RV and velocity dispersion estimates from H96, we sigma-clip the sample at $3\text{-}\sigma$ and reject five stars.

This leaves 59 candidate cluster members across 15 clusters: 11 stars in NGC 6838 (M 71); 8 stars in each of NGC 104 (47 Tuc) and NGC 6752; 7 stars in NGC 6397; 5 stars in each of NGC 5139 (ω Centauri), NGC 6121 (M 4) and NGC 6656 (M 22); 2 stars in each of NGC 6218 (M 12) and NGC 6254; and 1 star only in each of NGC 4833, NGC 5272 (M 3), NGC 6362, NGC 6723 (M 19), NGC 6779 (M 56), and NGC 6809.

We provide the TGAS and Tycho2 properties of these stars in Table 2, along with known radial velocities, and the likelihoods calculated in Section 2.3.

2.5. Photometry

Many of the identified clusters are classified as disk or bulge clusters, so it is likely that some stars identified as possible members are disk or bulge stars along the line of sight to the cluster. Furthermore, it is likely that high reddening would have made cluster stars too faint for detection with Tycho2. So the next step is to assess whether the stars are photometrically consistent with their nearest cluster. To do this, we wish to investigate whether the identified stars are consistent with an old isochrone at the known distance, reddening, and metallicity.

⁵ We experimented with different likelihood cuts and found that the analysis is fairly insensitive to the precise likelihood cut value but that a cut at $\mathcal{L}_i > -11$ works well.

Once again, we cross-match with the Tycho2 catalogue to extract B_T and V_T magnitudes, which are very close to the Johnson B and V magnitudes. We then extract representative isochrones for each cluster from the Dartmouth Stellar Evolution Database (Dotter et al. 2008). To do this, we assume an α -element abundance $[\alpha/\text{Fe}]$ of 0.2 dex and an age of 11 Gyr, and use $[\text{Fe}/\text{H}]$ metallicities from H96 rounded to the nearest 0.5 dex. We adjust the isochrone magnitudes for distance (using distance moduli calculated from distances in H96), and correct the observed magnitudes for extinction using reddening values from H96 and extinction coefficients from Sirianni et al. (2005), using the F435W filter to approximate B_T and the F555W filter to approximate V_T .⁶

In Figure 1, we show distance-corrected isochrones for each cluster. The solid lines show the isochrone with cluster $[\text{Fe}/\text{H}]$, the dashed lines show the isochrones at ± 0.5 dex, and the dotted lines show the isochrones at ± 1 dex. The TGAS stars identified as possible members are shown as coloured points, with their colours representing their likelihood of membership based on their position, parallax and PM, from orange (high) to blue (low). TGAS stars already ruled out as members (and so likely MW foreground stars) are shown in black.

From a visual inspection of the resulting isochrones for each cluster, we find that the candidate cluster members in NGC 4833, NGC 6362, NGC 6723 and NGC 6779 are all significantly offset from the isochrones and so we remove these from further consideration. We also reject 1 star in NGC 6254, 2 stars in NGC 6656, 1 star in NGC 6752, and 3 stars in NGC 6838 that are all significantly bluer than the expected cluster isochrones. The other stars remain promising candidates, and we still have 48 possible members across 11 clusters.

2.6. Besançon Simulations

As a final test, we wish to compare the velocities of the TGAS stars against predictions from the Besançon simulations (Robin et al. 2003); these simulations serve as a prediction for what the population of field stars should look like – both photometrically and kinematically – along the line of sight to any given cluster.

We selected stars from the Besançon simulations using the webtool provided, and we found that all of the default inputs were suitable for our purposes. We used the small-field option to select stars, and used Galactic longitudes and latitudes from H96 to identify the cluster centres.

In Figure 2 and Figure 3, we show 2D projections of the parallax, RA PM and Dec PM space for the 11 remaining clusters. The red star indicates the H96 distance inverted to calculate a parallax and the PMs from CD13. The coloured points are the candidate cluster members from TGAS, coloured according to their probability of membership from orange (high) to blue (low). The black points are TGAS stars selected inside $2R_{\text{tidal}}$ rejected as cluster member candidates (and so likely MW field stars). The grey points show the predictions for the MW field population from Besançon simulations. Note that the error bars are not aligned with the axes as we have incorporated the correlation terms in the five-parameter astrometric solution provided in the TGAS catalogue. The error bars show the major and minor axes of the 2D projection of the full covariance matrix. In the top-right corners, we show sky posi-

⁶ These approximations are sufficient for present analysis that does not rely on accurate photometry.

Table 2
TGAS star properties and membership selection statistics.

GID	α	δ	ϖ	$\mu_{\alpha*}$	μ_{δ}	B_T	V_T	v_r	Cluster	$\log \mathcal{L}_{\alpha\delta,i}$	$\log \mathcal{L}_{\varpi\mu,i}$	$\log \mathcal{L}_i$	
(1)	(2)	(3)	(4)	(5)	(6)	(7)	(8)	(9)	(10)	(11)	(12)	(13)	
	(deg)		(mas)	(mas/yr)		(mag)		(km/s)					
4689620330317403136	5.91	-72.28	0.274	4.22	-2.73	13.82	12.01	...	NGC 104	-0.204	-2.478	-2.683	*
4690024022888359424	7.30	-71.82	0.109	3.96	-1.60	13.64	11.72	-19.28	NGC 104	-6.887	-3.748	-10.634	
4689638437899435136	5.57	-72.10	0.580	2.09	-1.14	13.28	12.20	...	NGC 104	-0.814	-3.447	-4.260	
4689645000616682240	6.01	-71.93	0.757	4.01	-3.32	13.28	11.65	-30.57	NGC 104	-0.093	-3.006	-3.099	*
4689595831823970304	5.41	-72.41	0.675	4.24	-3.25	13.54	12.00	...	NGC 104	-1.944	-3.268	-5.212	
5843733808608717952	195.21	-71.07	0.210	-7.29	-0.56	13.18	12.41	...	NGC 4833	-3.216	-2.028	-5.244	
6083684354306876160	201.02	-47.65	-0.538	-13.52	-2.30	13.02	11.44	...	NGC 5139	-1.486	-8.313	-9.798	
6083671366325791488	201.46	-47.74	1.166	4.66	-0.73	12.39	11.50	257.09	NGC 5139	-0.395	-6.163	-6.558	
6083447684430417536	202.19	-47.82	1.065	1.35	-3.35	13.71	11.79	...	NGC 5139	-1.118	-6.499	-7.617	
608387730916697600	202.47	-47.49	1.383	-2.59	-1.87	12.97	11.46	...	NGC 5139	-1.851	-9.084	-10.935	
6083765993045114240	201.41	-47.23	-0.641	-7.83	-6.15	12.70	11.64	236.65	NGC 5139	-0.429	-8.547	-8.976	
1454784965950282240	205.46	28.39	0.225	-0.69	-2.85	14.74	12.46	-148.86	NGC 5272	-0.062	-0.939	-1.001	*
6045476290889048704	245.82	-26.54	0.586	-12.78	-18.38	14.13	11.65	69.90	NGC 6121	-0.017	-2.094	-2.111	*
6045490618893190656	246.01	-26.40	0.521	-13.41	-18.88	12.86	10.94	66.26	NGC 6121	-0.078	-2.061	-2.138	*
6045452204710238080	245.86	-26.79	0.810	-10.95	-17.14	12.93	10.91	...	NGC 6121	-0.189	-5.091	-5.280	*
4378870169323203328	252.05	-2.15	0.494	-1.47	-5.92	13.77	12.30	...	NGC 6218	-2.398	-4.878	-7.276	
4379054715477604864	251.67	-2.19	0.527	-4.51	-6.21	13.39	11.91	...	NGC 6218	-1.845	-7.584	-9.429	
4365636309932242432	254.23	-4.04	0.110	-3.41	-5.84	13.05	12.04	...	NGC 6254	-0.153	-4.879	-5.033	
4365621535247048960	254.30	-4.14	0.225	-4.22	-6.15	12.88	12.41	...	NGC 6254	-0.031	-3.727	-3.758	
5813186111412913280	262.91	-66.74	1.027	-2.82	-1.68	13.08	11.97	...	NGC 6362	-3.596	-6.550	-10.146	
5921742474972627456	265.18	-53.83	0.317	2.28	-18.92	11.92	10.54	...	NGC 6397	-0.731	-5.469	-6.200	*
5921747938171016320	265.08	-53.70	-0.150	3.45	-17.91	11.79	10.18	...	NGC 6397	-0.260	-4.060	-4.319	*
5921745567349079424	265.11	-53.80	0.441	2.04	-19.45	12.64	12.06	...	NGC 6397	-0.587	-5.876	-6.463	*
5921729074674635776	265.47	-53.56	0.159	3.79	-17.58	12.06	10.68	...	NGC 6397	-2.945	-7.572	-10.517	*
5921744708355615616	265.18	-53.75	0.098	4.61	-17.91	11.96	10.55	...	NGC 6397	-0.148	-6.352	-6.500	*
5921751030547464960	265.24	-53.66	-0.041	3.14	-16.24	12.41	11.20	23.21	NGC 6397	-0.120	-8.766	-8.887	*
5921744570916663040	265.16	-53.76	0.608	1.95	-17.19	11.77	10.54	...	NGC 6397	-0.202	-4.154	-4.357	*
4077494753703271424	279.04	-23.92	0.585	6.98	-5.99	12.31	11.09	-130.00	NGC 6656	-0.023	-4.215	-4.238	*
4076740385647365376	279.04	-24.10	0.433	10.31	-4.17	13.12	11.47	...	NGC 6656	-0.285	-5.788	-6.073	*
4077552649862421248	278.49	-23.91	0.609	8.30	-1.32	12.16	12.03	...	NGC 6656	-2.650	-4.648	-7.298	
4077590892251201152	279.15	-23.81	0.837	5.52	-4.94	11.91	11.84	...	NGC 6656	-0.085	-4.411	-4.497	
4076708431092287104	279.21	-24.53	0.533	3.28	-5.00	13.84	11.39	...	NGC 6656	-2.874	-6.778	-9.652	
6731282993530282368	285.05	-36.46	0.593	10.93	12.18	13.56	12.04	...	NGC 6723	-3.475	-7.213	-10.687	
6638364227941381120	288.71	-59.69	0.406	1.08	-0.53	12.72	12.62	...	NGC 6752	-2.659	-6.079	-8.738	
6638371821443555200	289.15	-59.58	0.619	-1.20	-2.29	12.79	11.21	-22.66	NGC 6752	-5.514	-2.892	-8.406	
6638358730383247872	288.79	-59.83	0.308	-1.04	-8.24	13.40	11.48	...	NGC 6752	-2.924	-6.298	-9.221	
6632379757949812864	286.99	-60.12	0.259	-3.50	-5.34	13.16	10.97	...	NGC 6752	-1.372	-8.576	-9.948	
6440142622417461888	288.00	-60.59	0.447	-2.10	-4.41	13.39	11.15	...	NGC 6752	-1.107	-3.081	-4.188	
6638306159983484544	288.02	-60.38	0.390	-3.01	-7.24	13.08	11.16	...	NGC 6752	-0.632	-8.169	-8.800	
6632375291182475904	287.55	-60.01	0.360	-3.50	-4.38	13.96	12.11	...	NGC 6752	-0.070	-10.118	-10.188	
6632371236733360640	287.68	-60.09	0.493	-4.08	-5.79	14.19	12.94	...	NGC 6752	-0.030	-10.290	-10.321	
2039266037106291840	289.11	30.39	0.674	1.27	1.25	12.74	12.98	...	NGC 6779	-2.960	-6.188	-9.148	
6751300358628240384	294.80	-30.89	1.230	-6.08	-8.48	12.60	11.54	...	NGC 6809	-1.395	-8.582	-9.977	
1821415194086555520	298.60	18.63	-0.660	1.35	-4.31	13.44	12.52	...	NGC 6838	-4.282	-4.175	-8.457	
1821415709482628608	298.65	18.66	-0.600	2.13	-1.50	13.56	12.71	...	NGC 6838	-5.064	-5.849	-10.914	
1821605993716534784	298.34	18.66	-0.042	0.42	-4.20	12.82	12.96	...	NGC 6838	-2.311	-3.273	-5.583	
1821618912978148736	298.32	18.75	1.161	-6.19	-6.46	13.54	11.87	...	NGC 6838	-1.517	-4.949	-6.466	
1821580911107536640	298.30	18.56	0.621	-0.85	-5.44	11.79	11.59	...	NGC 6838	-6.092	-4.266	-10.357	
1821603279296706688	298.62	18.67	1.056	-4.50	-5.62	13.67	11.72	...	NGC 6838	-4.112	-4.094	-8.206	
1821607780422917376	298.54	18.75	0.818	-2.45	-5.61	11.72	11.30	...	NGC 6838	-1.010	-4.134	-5.144	
1821618294502862592	298.32	18.72	1.365	-5.93	-6.34	13.32	12.04	...	NGC 6838	-1.750	-5.795	-7.546	
1821615408284919552	298.55	18.86	0.521	-4.58	-9.49	13.17	12.21	...	NGC 6838	-1.756	-7.184	-8.940	
1821621489958617600	298.34	18.83	1.289	-3.44	-9.39	13.52	11.47	...	NGC 6838	-1.186	-7.957	-9.143	
1821626953157011072	298.46	18.86	-0.181	-2.90	-2.31	14.13	11.79	...	NGC 6838	-0.693	-5.020	-5.713	

Notes. Columns: (1) *Gaia* ID; (2) Right Ascension; (3) Declination; (4) parallax; (5) PM in Right Ascension; (6) PM in Declination; (7) Tycho2 B magnitude; (8) Tycho2 V magnitude; (9) radial velocity from RAVE; (10) nearest cluster centre; (11) logarithm of position likelihood; (12) logarithm of parallax and PM likelihood; (13) logarithm of total likelihood. Stars marked * are those we identify as cluster members and use in Section 3 to derive the cluster properties in Table 3. Uncertainties and correlations are not listed, but are available from the TGAS, Tycho2 and RAVE catalogues.

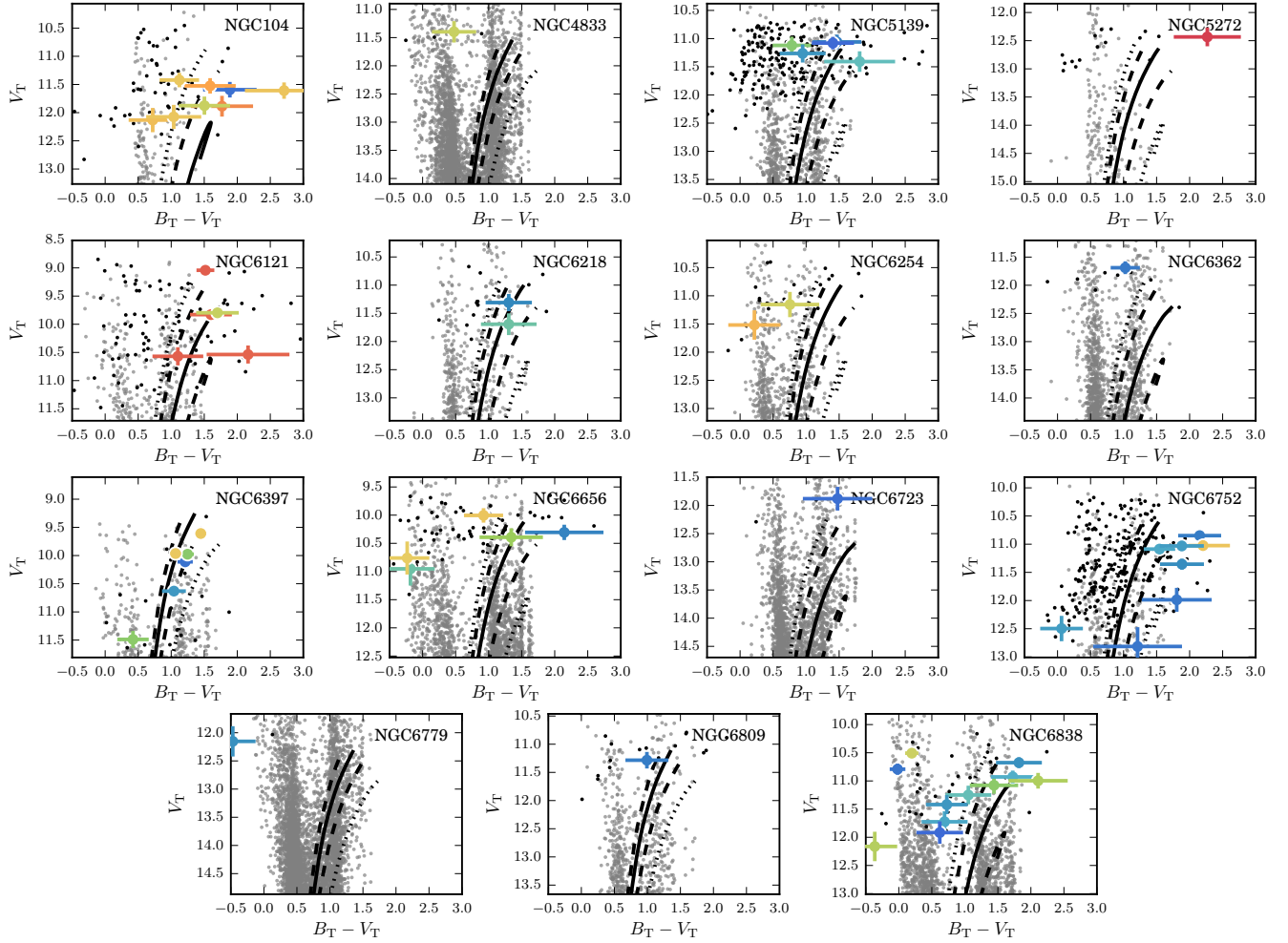


Figure 1. Representative distance-corrected isochrones for the GCs with candidate members in TGAS. The solid lines show an 11 Gyr, $[\alpha/\text{Fe}]=0.2$ dex isochrone with $[\text{Fe}/\text{H}]$ metallicity from H96 rounded to the nearest 0.5 dex, the dashed lines show the isochrones at ± 0.5 dex, and the dotted lines show the isochrones at ± 1 dex. The extinction-corrected TGAS cluster member candidates are shown as coloured points where the colour indicates their likelihood from high (orange) to low (blue). The black points are TGAS stars ruled out as cluster members. For comparison, we show the expected MW field star population from Besançon model predictions as grey points.

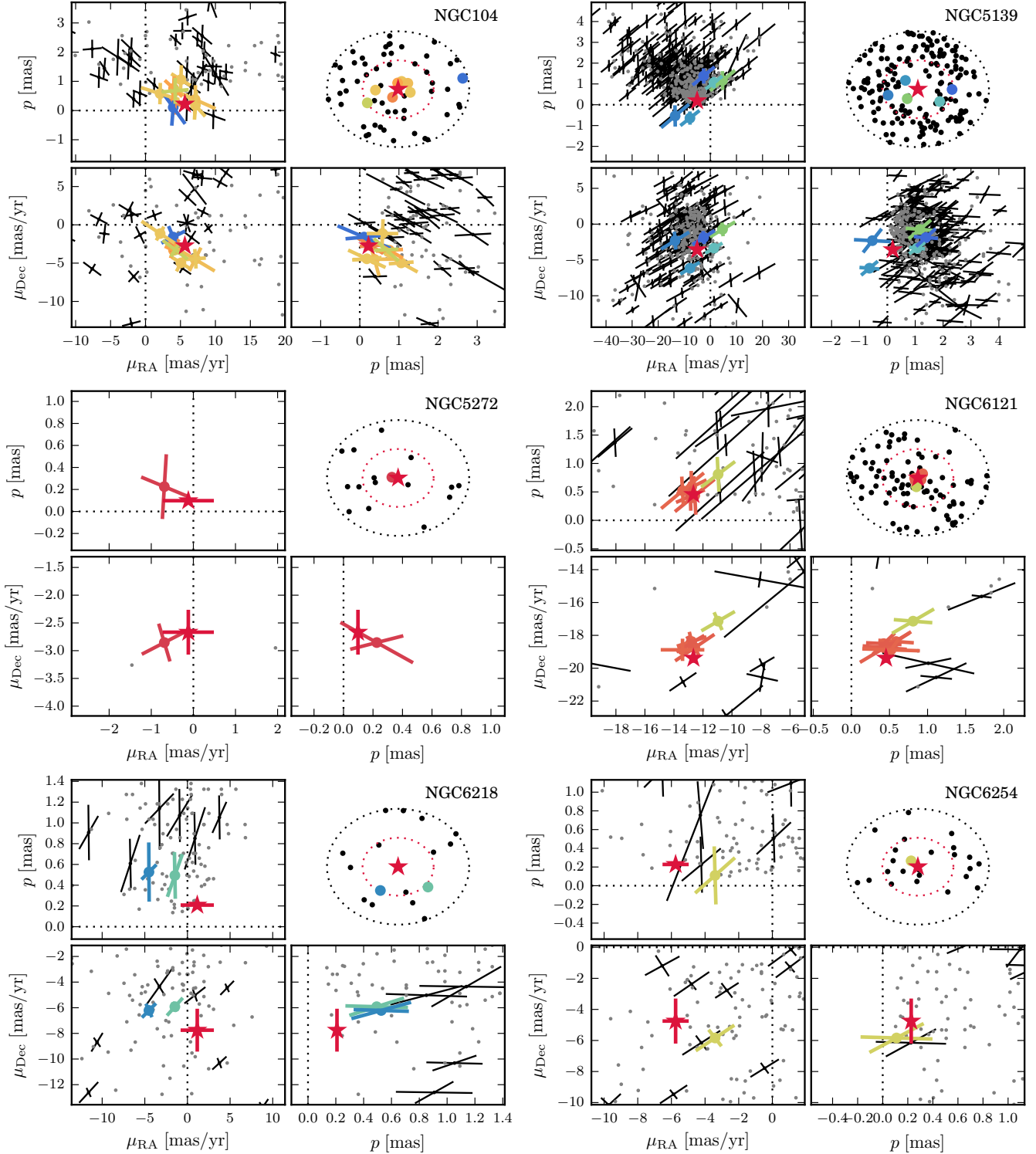


Figure 2. Sky positions, parallaxes, and proper motions for the TGAS stars in NGC 104, NGC 5139, NGC 5272, NGC 6121, NGC 6218, and NGC 6254. The top-right panels in each set show the sky positions of the TGAS stars identified within $2R_{\text{tidal}}$ relative to the cluster centre (red star). The red dotted line marks R_{tidal} and the black dotted line marks $2R_{\text{tidal}}$. The remaining panels show projections of the five-parameter astrometric solution for parallax, RA PM and Dec PM. The literature values we used to determine membership probabilities (parallaxes from inverted distances from H96 and PMs from CD13) are shown as red stars. The TGAS cluster member candidates are shown as coloured points, coloured by their probability of membership from orange (high) to blue (low). The black points are TGAS stars rejected as cluster members, and thus, thought to be MW field stars. For comparison, Besançon model predictions are shown as grey points. In some cases, most of the Besançon stars fall outside of the plot limits.

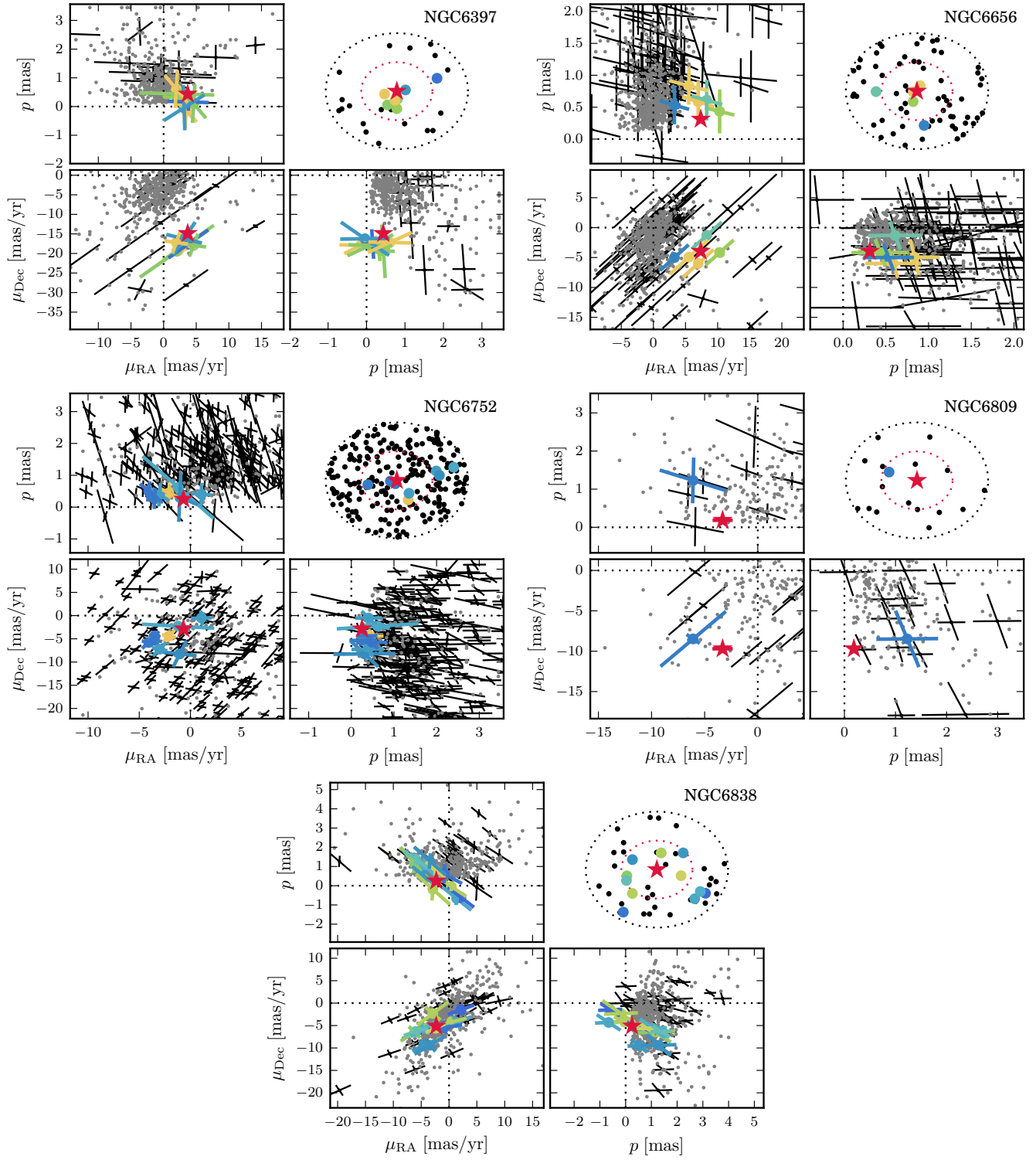


Figure 3. Same as Figure 2 for NGC 6397, NGC 6656, NGC 6752, NGC 6809, and NGC 6838.

tion maps for the TGAS candidate cluster members (coloured points) and the TGAS field stars (black points) relative to the centre of the cluster (red star). The red dotted lines marks the tidal radii R_{tidal} , and the black dotted lines mark $2R_{\text{tidal}}$.

We find that both the photometric and kinematic properties for 6 of the remaining 11 clusters are consistent with the Besançon predictions for the field-star population, and the other TGAS stars in the respective fields, which are also assumed to be field stars. In all cases, we cannot be confident that we have truly selected cluster members and not field stars, and so we remove these clusters from further consideration. They are: NGC 5139, NGC 6218, NGC 6254, NGC 6752, NGC 6809, and NGC 6838.

Thus we are left with 5 promising clusters, which we now discuss in turn.

NGC 104 has 8 candidate stars, but it also poses the challenge that the Besançon model predictions overlap the part of parallax and PM space where NGC 104 stars are expected. Therefore, for this cluster we decided to restrict our final analysis to only the stars within $0.5R_{\text{tidal}}$ from the centre, which is where the cluster-to-foreground star ratio should be largest. There are 5 stars that meet this criterion, and all of them clump in PM space around the expected NGC 104 PM value. While we cannot strictly rule out that any of these 5 stars are foreground, we can rule out that a significant fraction of them are foreground, since the Besançon models predict a much larger PM dispersion for such stars. One of the 5 candidate member stars also has an RV estimate within 3σ of the cluster value (in fact, at 1.2σ). This does lend further credence to their membership (although we find that 65% of the Besançon stars also have RVs predicted to be within 3σ of the cluster value).

NGC 5272 has only a single candidate, however it is very close to the cluster centre and the agreement in PM and parallax is excellent. Furthermore, both cluster and star sit far away from the Besançon predictions. We believe this star is a member of NGC 5272, though we acknowledge that it is hard to be certain for a single star.

NGC 6121 has five candidates; all lie well within the tidal radius and all have PMs and parallaxes consistent both with the cluster and each other, and inconsistent with the Besançon predictions. We note that one star (green) is slightly offset from the others, however its proximity to the centre and its position relative to a cluster isochrone both mark it as a promising candidate. Unfortunately, this offset star is not augmented by RV data, however two other candidates do have RV estimates: one lies at $\sim 0.2\sigma$ from the cluster value and the other at $\sim 1.1\sigma$ from the cluster value, thus indicating that they are indeed bona fide cluster members. We believe all 5 stars are cluster members.

NGC 6397 has 7 candidates, all of which are clearly offset from the bulk of the Besançon predictions in PM. One star (light blue) also has an RV measurement within 1σ of the cluster measurement, however, $\sim 22\%$ of the Besançon stars have RVs within 3σ of the cluster value, so RV is not a strong indicator of cluster membership. Nevertheless, we believe that all 7 stars are members.

NGC 6656 has three candidates, all of which have parallaxes and μ_δ measurements consistent with the Besançon population; two (yellow and green) are clearly offset in μ_{α^*} from the bulk of the background predictions but the third (blue) does sit at the edge of the predicted background distribution; as this star also sits outside of the tidal radius and is somewhat redward of the expected cluster isochrones, we remove it from our analysis. Of the remaining two stars, the star coloured yellow

has an RV measurement that is 2σ offset from the cluster value. Fewer than 3% of the Besançon stars have RVs within 3σ of the cluster velocity, so RV is indeed a strong indicator of cluster membership for this cluster. We believe that the remaining two stars are members.

In summary, we are confident that we have identified 20 GC member stars: 5 stars in NGC 104, one star in NGC 5272, 5 stars in NGC 6121, 7 stars in NGC 6397, and 2 stars in NGC 6656.

Perhaps unsurprisingly, NGC 6121, NGC 6397 and NGC 6656 are 3 of the 4 closest clusters.⁷ Thanks in part to their proximity, these clusters are among the best studied and so precise measurement of both their distances (parallaxes) and their absolute PMs are extremely valuable to aid our understanding of their nature and origins.

3. PROPER MOTIONS AND PARALLAXES

With just a single star in NGC 5272, there is little more we can do here; however, for the other clusters we can combine the TGAS estimates and uncertainties to calculate weighted average parallaxes and PMs for the clusters. To do this, we perform a Monte Carlo sampling using the member stars identified in TGAS to estimate the cluster PM and parallax along with their covariance. The results are presented in Table 3, and compared in the following subsections to results from previous studies.

Comparing our parallax estimate to previous measurements is subtly non-trivial as usually previous studies have estimated distances or distance moduli, so two types of measurement (along with their uncertainties) must be converted into the third type for comparison. The choice of which measurement type to use for comparison is somewhat arbitrary, and we choose to compare distances here, as cluster distances are commonly the quantity that we wish to know.

3.1. NGC 104 (47 Tucanae)

For NGC 104, we find parallax $\varpi = 0.531 \pm 0.210$ mas, RA PM $\mu_{\alpha^*} = 5.50 \pm 0.70$ mas/yr, and Dec PM $\mu_\delta = -3.99 \pm 0.55$ mas/yr, with correlation terms $\rho(\varpi, \mu_{\alpha^*}) = -0.440$, $\rho(\varpi, \mu_\delta) = -0.503$, and $\rho(\mu_{\alpha^*}, \mu_\delta) = -0.332$. In Figure 4, the upper and middle panels show the parallaxes and PMs of the 5 TGAS stars (black) and our averages (red).

There are five previous PM estimates for NGC 104: [Cudworth & Hanson \(1993\)](#) measured $\mu_{\alpha^*} = 3.4 \pm 1.7$ mas/yr and $\mu_\delta = -1.9 \pm 1.5$ mas/yr from the ground; [Odenkirchen et al. \(1997\)](#) measured $\mu_{\alpha^*} = 7.0 \pm 1.0$ mas/yr and $\mu_\delta = -5.3 \pm 1.0$ mas/yr using *Hipparcos* data; [Freire et al. \(2003\)](#) measured $\mu_{\alpha^*} = 5.3 \pm 0.6$ mas/yr and $\mu_\delta = -3.3 \pm 0.6$ mas/yr using radio observations of millisecond pulsars (MSPs); [Anderson & King \(2003\)](#) measured $\mu_{\alpha^*} = 5.88 \pm 0.18$ mas/yr and $\mu_\delta = -2.53 \pm 0.18$ mas/yr using *HST*/WFPC2⁸; and [Cioni et al. \(2016\)](#) measured $\mu_{\alpha^*} = 7.26 \pm 0.03$ mas/yr and $\mu_\delta = -1.25 \pm 0.03$ mas/yr using ground-based data from VISTA. These points are shown in the PM panel (centre left) of Figure 4 as orange, green, cyan, blue and purple points respectively.

⁷ The fourth cluster is NGC 6544, which was excluded from our analysis as it has no stars inside $2R_{\text{tidal}}$ that passed the distance and extinction test in Section 2.2.

⁸ We did not use the absolute PM given in [Anderson & King \(2003\)](#); instead we used their measured motion of NGC 104 relative to the Small Magellanic Cloud (SMC) combined with the SMC PM measurement from [Kalliyayil et al. \(2006\)](#).

Table 3
TGAS parallax and proper motion results.

Cluster	ϖ	$\mu_{\alpha*}$	μ_{δ}	$\sigma\varpi$	$\sigma\mu_{\alpha*}$	$\sigma\mu_{\delta}$	$\rho(\varpi, \mu_{\alpha*})$	$\rho(\varpi, \mu_{\delta})$	$\rho(\mu_{\alpha*}, \mu_{\delta})$
(1)	(2)	(3)	(4)	(5)	(6)	(7)	(8)	(9)	(10)
NGC 104	0.531	5.50	-3.99	0.210	0.70	0.55	-0.440	-0.503	-0.332
NGC 5272	0.225	-0.69	-2.85	0.289	0.51	0.37	-0.197	-0.593	0.319
NGC 6121	0.556	-12.51	-18.33	0.149	0.50	0.29	0.589	0.519	0.488
NGC 6397	0.205	3.03	-17.88	0.223	1.09	1.36	-0.066	0.036	0.755
NGC 6656	0.509	8.64	-5.09	0.222	1.49	1.45	-0.194	-0.160	0.935

Notes. Columns: (1) cluster name; (2) parallax estimate; (3) RA PM estimate; (4) Dec PM estimate; (5) uncertainty on parallax estimate; (6) uncertainty on RA PM estimate; (7) uncertainty on Dec PM estimate; (8) correlation between parallax and RA PM estimates; (9) correlation between parallax and Dec PM estimates; (10) correlation between RA PM and Dec PM estimates.

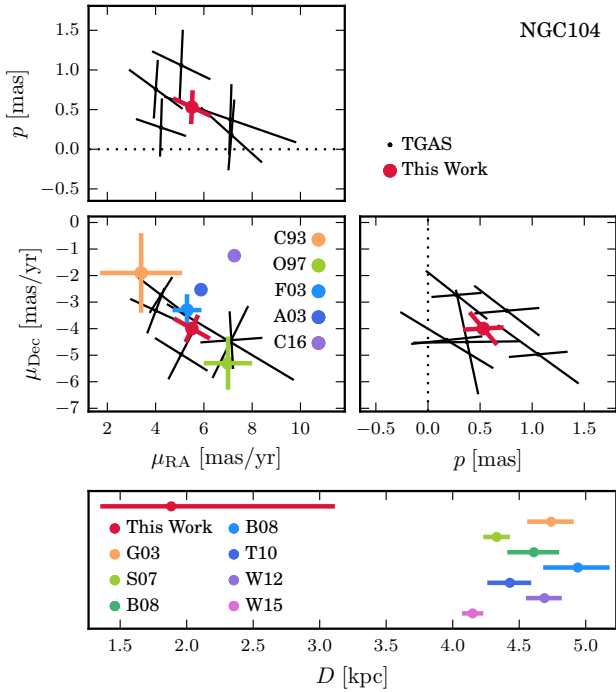


Figure 4. Upper and middle panels: Parallax and PM results for NGC 104. The black points show the 5 TGAS stars we identified as cluster members. The red points shows the mean values we have calculated here. In the PM plot (middle left) we compare our estimate to values from [Cudworth & Hanson \(1993\)](#) (orange, ground-based), [Odenkirchen et al. \(1997\)](#) (green, *Hipparcos*), [Freire et al. \(2003\)](#) (cyan, millisecond pulsars), [Anderson & King \(2003\)](#) (blue, *HST*), and [Cioni et al. \(2016\)](#) (purple, VISTA). Our PM estimate is consistent with both the estimate from MSP timing and the estimate from *HST* astrometry. Lower panel: Distance comparison for NGC 104. We invert our parallax measurement to obtain a distance estimate (red). We also show previous distance estimates from [Gratton et al. \(2003\)](#) (orange, MS fitting), [Salaris et al. \(2007\)](#) (light green, HB fitting), [Bono et al. \(2008\)](#) (dark green, TRGB), cyan RR Lyraes), [Thompson et al. \(2010\)](#) (blue, eclipsing binary), [Woodley et al. \(2012\)](#) (purple, WD SEDs), and [Watkins et al. \(2015a\)](#) (pink, dynamical). Our distance is considerably smaller than previous estimates.

Our PM estimate shows best agreement with the estimate derived from MSP timing by [Freire et al. \(2003\)](#) and the *HST* measurement by [Anderson & King \(2003\)](#); for the latter our RA PM is in very good agreement, though our Dec PM is slightly larger than theirs.

Our parallax of $\varpi = 0.531 \pm 0.210$ mas corresponds to a distance of $D = 1.88^{+1.23}_{-0.53}$ kpc. NGC 104 is one of the best studied Galactic GCs and so there are many estimates of its distance in the literature; for a complete overview of previ-

ous distance determinations, see Table 2 of [Woodley et al. \(2012\)](#). Here we compare with only a subset of these chosen to cover a wide variety of estimation methods: [Gratton et al. \(2003\)](#) estimated $D = 4.74^{+0.18}_{-0.17}$ kpc via main-sequence (MS) fitting; [Salaris et al. \(2007\)](#) estimated $D = 4.33 \pm 0.10$ kpc via horizontal branch (HB) fitting; [Bono et al. \(2008\)](#) estimated $D = 4.61^{+0.20}_{-0.19}$ kpc using the tip of the Red Giant Branch (TRGB) and $D = 4.94^{+0.26}_{-0.24}$ kpc using RR Lyraes; [Thompson et al. \(2010\)](#) estimated $D = 4.43^{+0.17}_{-0.16}$ kpc using an eclipsing binary; [Woodley et al. \(2012\)](#) estimated $D = 4.69^{+0.14}_{-0.13}$ kpc using white dwarf (WD) spectral energy distributions (SEDs); and [Watkins et al. \(2015a\)](#) used estimated $D = 4.15 \pm 0.08$ kpc using stellar kinematics. We show these distance estimates along with our own in the lower panel of Figure 4. Our distance estimate is considerably smaller than all of the previous distance estimates for NGC 104.

NGC 104 is the only cluster of the five in our sample for which the TGAS distance estimate is not consistent at 1σ with literature estimates. It is possible that this reflects some level of foreground contamination in our sample of five stars. Three of the stars have individual parallax estimates consistent with the known NGC 104 distance, while the other two do not (see Figure 4, top-left and middle-right panels).

3.2. NGC 5272 (*M 3*)

For NGC 5272, we have only one member star so we do not perform a Monte Carlo sampling but instead report the TGAS values for the single member star. The TGAS estimate finds parallax $\varpi = 0.225 \pm 0.289$ mas, RA PM $\mu_{\alpha*} = -0.69 \pm 0.51$ mas/yr, and Dec PM $\mu_{\delta} = -2.85 \pm 0.37$ mas/yr, with correlation terms $\rho(\varpi, \mu_{\alpha*}) = -0.197$, $\rho(\varpi, \mu_{\delta}) = -0.593$, and $\rho(\mu_{\alpha*}, \mu_{\delta}) = 0.319$. In Figure 5, the upper and middle panels show the parallax and PMs of the identified TGAS star.

There are 5 previous PM estimates for NGC 5272; unfortunately all are ground-based estimates and there are no *HST* measurements for comparison. They are: [Cudworth & Hanson \(1993\)](#) measured $\mu_{\alpha*} = -1.2 \pm 2.5$ mas/yr and $\mu_{\delta} = 2.4 \pm 3.0$ mas/yr from the ground; [Scholz et al. \(1993\)](#) measured $\mu_{\alpha*} = -3.1 \pm 0.2$ mas/yr and $\mu_{\delta} = -2.3 \pm 0.4$ mas/yr using photographic plates; [Odenkirchen et al. \(1997\)](#) measured $\mu_{\alpha*} = 0.9 \pm 1.0$ mas/yr and $\mu_{\delta} = -2.2 \pm 1.0$ mas/yr using *Hipparcos* data; [Geffert \(1998\)](#) measured $\mu_{\alpha*} = -1.2 \pm 0.8$ mas/yr and $\mu_{\delta} = -3.2 \pm 0.8$ mas/yr also using *Hipparcos* stars; and [Wu et al. \(2002\)](#) measured $\mu_{\alpha*} = -0.06 \pm 0.3$ mas/yr and $\mu_{\delta} = -2.6 \pm 0.3$ mas/yr using photographic plates spanning a 70 year baseline. The latter four points are shown in the PM panel (centre left) of Figure 5 as orange, green, cyan, and

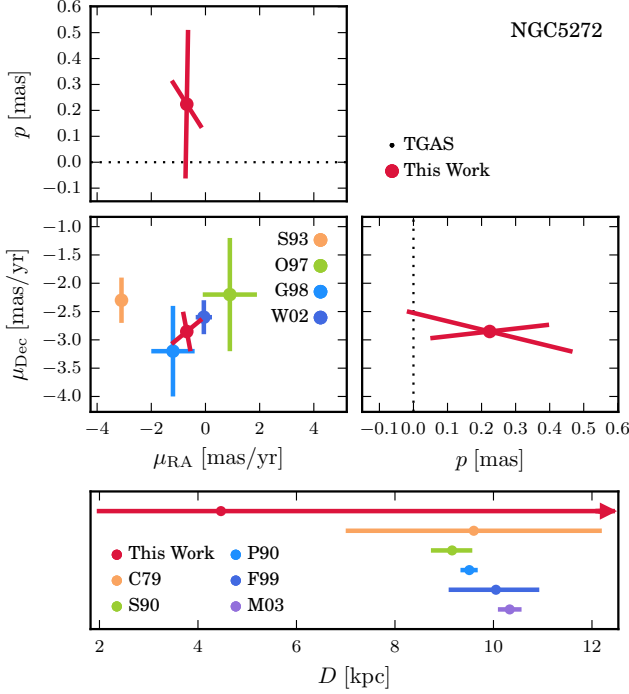


Figure 5. Upper and middle panels: Parallax and PM results for NGC 5272. The black points show the TGAS star we identified as a cluster member. In the PM plot (middle left) we compare our estimate to values from Scholz et al. (1993) (orange, photographic plates), Odenkirchen et al. (1997) (green, *Hipparcos*), Geffert (1998) (cyan, *Hipparcos*), and Wu et al. (2002) (blue, photographic plates). Our PM estimate is consistent with both the latter two estimates. (There is a further estimate given by Cudworth & Hanson (1993) however this is not shown as it does not lie within the plot limits.) Lower panel: Distance comparison for NGC 5272. We invert our parallax measurement to obtain a distance estimate (red). We also show previous distance estimates from Cudworth (1979) (orange, dynamical), Sandage & Cacciari (1990) (green, MS fitting), Paez et al. (1990) (cyan, CMD fitting), Ferraro et al. (1999) (blue, HB fitting), and Marconi et al. (2003) (purple, RR Lyrae pulsations). Our distance is considerably smaller than previous estimates.

blue points respectively. The estimate by Cudworth & Hanson (1993) is not shown as it is significantly offset from the others and is not located within the plot limits. The TGAS PM estimate shows best agreement with the estimate derived using photographic plates by Wu et al. (2002) and the *Hipparcos* measurement by Geffert (1998).

Our parallax of $\varpi = 0.225 \pm 0.289$ mas corresponds to a distance of $D = 4.44^{+\infty}_{-2.50}$ kpc. The upper error bar on the distance is unconstrained as the lower error bar on the parallax extends below zero, which, as previously discussed, is unphysical but statistically rigorous. NGC 5272 has a number of previous estimates of its distance in the literature; here we compare with only a subset of these chosen to cover a wide variety of estimation methods: Cudworth (1979) estimated $D = 9.6 \pm 2.6$ kpc from cluster kinematics; Sandage & Cacciari (1990) estimated $D = 9.16^{+0.43}_{-0.41}$ kpc via main-sequence fitting; Paez et al. (1990) estimated $D = 9.51^{+0.18}_{-0.17}$ kpc using colour-magnitude diagram fitting; Ferraro et al. (1999) estimated $D = 10.05^{+0.97}_{-0.88}$ kpc using HB fitting; and Marconi et al. (2003) estimated $D = 10.33 \pm 0.24$ kpc using RR Lyrae pulsations. We show these distance estimates along with our own in the lower panel of Figure 5. Our distance estimate is considerably smaller than all of the previous distance estimates for NGC 5272.

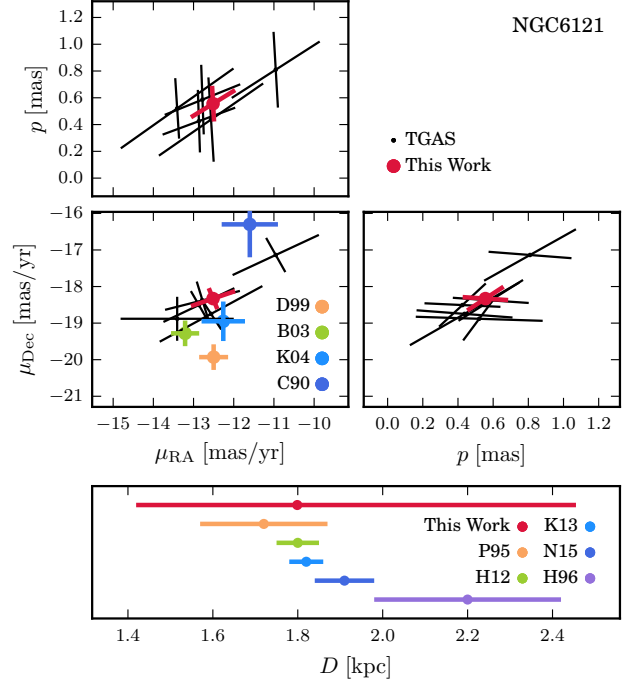


Figure 6. Upper and middle panels: Parallax and PM results for NGC 6121. The black points show the 5 TGAS stars we identified as cluster members. The red points shows the mean values we have calculated here. In the PM plot (middle left) we compare our estimate to values from Dinescu et al. (1999a) (orange, ground-based), Bedin et al. (2003) (green, *HST*), Kalirai et al. (2004) (cyan, *HST*), and Cudworth & Rees (1990) (blue, ground-based). The PMs we measure are consistent with the previous *HST* measurements and have similar uncertainties. Lower panel: Distance comparison for NGC 6121. We invert our parallax measurement to obtain a distance estimate (red). We also show previous distance estimates from Peterson et al. (1995) (orange, dynamical), Hendricks et al. (2012) (green, HB luminosity), Kaluzny et al. (2013) (cyan, eclipsing binaries), Neeley et al. (2015) (blue, RR Lyraes), and the estimate from H96 (purple). Our distance is consistent with previous estimates within our uncertainties, but our uncertainties are not yet competitive with existing results.

3.3. NGC 6121 (M4)

For NGC 6121, we find parallax $\varpi = 0.556 \pm 0.149$ mas, RA PM $\mu_{\alpha*} = -12.51 \pm 0.50$ mas/yr, and Dec PM $\mu_{\delta} = -18.33 \pm 0.29$ mas/yr, with correlation terms $\rho(\varpi, \mu_{\alpha*}) = 0.589$, $\rho(\varpi, \mu_{\delta}) = 0.519$, and $\rho(\mu_{\alpha*}, \mu_{\delta}) = 0.488$. In Figure 6, the upper and middle panels show the parallaxes and PMs of the 5 TGAS stars (black) and our averages (red).

To define membership probabilities in Section 2.3, we used the PM from CD13 as a reference. In fact, the PM for NGC 6121 given in that catalogue is a combination of three separate studies and so we compare our PM again each of those studies here: Dinescu et al. (1999a) measured $\mu_{\alpha*} = -12.50 \pm 0.36$ mas/yr and $\mu_{\delta} = -19.93 \pm 0.35$ mas/yr from SPM photographic plates using *Hipparcos* stars as a reference frame; Bedin et al. (2003) measured $\mu_{\alpha*} = -13.21 \pm 0.35$ mas/yr and $\mu_{\delta} = -19.28 \pm 0.35$ mas/yr using *HST*/WFPC2 data; and Kalirai et al. (2004) measured $\mu_{\alpha*} = -12.26 \pm 0.54$ mas/yr and $\mu_{\delta} = -18.95 \pm 0.54$ mas/yr also using *HST*/WFPC2 but with a longer baseline. These points are shown in the PM panel (centre left) of Figure 6 as orange, green and cyan points respectively.

Our PM in RA is consistent with all three studies, but our PM in Dec is in much better agreement with the two *HST* PMs than the ground-based PM. *HST* tends to be less susceptible to various kinds of errors than ground-based measurements,

so the good agreement between the *HST* and TGAS estimates is very encouraging. This is also consistent with the conclusions from [van der Marel & Sahlmann \(2016\)](#) who recently studied rotation in the Large and Small Magellanic Clouds using TGAS and found excellent agreement between the TGAS estimates and earlier *HST* studies.

There is one further estimate of the PM of NGC 6121 which used bright field stars to create a reference frame to measure $\mu_{\alpha^*} = -11.6 \pm 0.7$ mas/yr and $\mu_{\delta} = -16.3 \pm 0.9$ mas/yr ([Cudworth & Rees 1990](#)) (shown in blue), which is significantly offset from the other previous studies and our own TGAS estimate.

Our parallax of $\varpi = 0.556 \pm 0.149$ mas corresponds to a distance of $D = 1.80^{+0.66}_{-0.38}$ kpc. This is in good agreement with the distance of $D = 2.2$ kpc from [H96](#), which we inverted to obtain a parallax for the membership probability analysis in [Section 2.3](#). As the closest GC, M4 has been well studied and so there are many estimates of its distance in the literature, and in fact the [H96](#) value is among the largest. We summarise a selection here covering a wide variety of estimation methods: [Peterson et al. \(1995\)](#) used PMs and LOS velocity dispersions to estimate a distance of $D = 1.72 \pm 0.14$ kpc; [Hendricks et al. \(2012\)](#) used the luminosity of the horizontal branch to measure $D = 1.80 \pm 0.05$ kpc; [Kaluzny et al. \(2013\)](#) used three eclipsing binaries in NGC 6121 to measure $D = 1.82 \pm 0.04$ kpc; and [Neeley et al. \(2015\)](#) used RR Lyraes to measure $D = 1.91 \pm 0.07$ kpc. We show these distance estimates along with our own in the lower panel of [Figure 6](#).

Our distance estimate is consistent with all previous estimates within their uncertainties, however, our distance uncertainty is considerably larger than the previous results.

3.4. NGC 6397

For NGC 6397, we find parallax $\varpi = 0.205 \pm 0.223$ mas, RA PM $\mu_{\alpha^*} = 3.03 \pm 1.09$ mas/yr, and Dec PM $\mu_{\delta} = -17.88 \pm 1.36$ mas/yr, with correlation terms $\rho(\varpi, \mu_{\alpha^*}) = -0.066$, $\rho(\varpi, \mu_{\delta}) = 0.036$, and $\rho(\mu_{\alpha^*}, \mu_{\delta}) = 0.755$. In [Figure 7](#), the upper and middle panels show the parallaxes and PMs of the 7 TGAS stars (black) and our averages (red).

There are four previous PM estimates for NGC 6397: [Cudworth & Hanson \(1993\)](#) measured $\mu_{\alpha^*} = 3.3 \pm 0.5$ mas/yr and $\mu_{\delta} = -15.2 \pm 0.6$ mas/yr from the ground; [Milone et al. \(2006\)](#) measured $\mu_{\alpha^*} = 3.39 \pm 0.15$ mas/yr and $\mu_{\delta} = -17.55 \pm 0.15$ mas/yr using *HST*/WFPC2 data; [Kalirai et al. \(2007\)](#) measured $\mu_{\alpha^*} = 3.56 \pm 0.04$ mas/yr and $\mu_{\delta} = -17.34 \pm 0.04$ mas/yr using a combination of *HST*/WFPC2 and *HST*/ACS data; and [CD13](#) measured $\mu_{\alpha^*} = 3.69 \pm 0.29$ mas/yr and $\mu_{\delta} = -14.88 \pm 0.26$ mas/yr using a combination of photographic plates and ground-based CCD images. These points are shown in the PM panel (centre left) of [Figure 7](#) as orange, green, cyan and blue points respectively. Note that all of these measurements are in reasonable agreement in μ_{α^*} , but are discrepant at ~ 2 mas/yr in μ_{δ} . We find that our μ_{δ} estimate is in much better agreement with the two *HST* PMs than the two ground-based PMs. This trend is consistent with our findings for NGC 6121 in [Section 3.3](#).

Our parallax of $\varpi = 0.205 \pm 0.223$ mas corresponds to a distance of $D = 4.88^{+\infty}_{-2.55}$ kpc. Our upper error bar on the distance is unconstrained as the lower error bar on the parallax for NGC 6397 extends below zero, which, as previously discussed, is unphysical but statistically rigorous.

There are a number of previous distance estimates in the literature, of which we show a representative sample here, obtained using different methods: [Reid & Gizis \(1998\)](#) es-

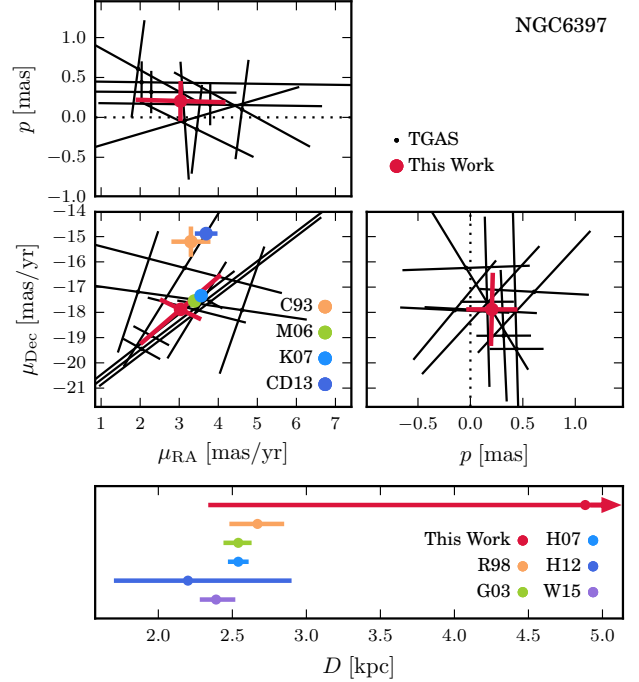


Figure 7. Upper and middle panels: Parallax and PM results for NGC 6397. The black points show the 7 TGAS stars we identified as cluster members. The red points shows the mean values we have calculated here. In the PM plot (middle left) we compare our estimate to values from [Cudworth & Hanson \(1993\)](#) (orange, ground-based), [Milone et al. \(2006\)](#) (green, *HST*), [Kalirai et al. \(2007\)](#) (cyan, *HST*), and [CD13](#) (blue, ground-based). The PMs we measure are consistent with the previous *HST* measurements, albeit with uncertainties an order of magnitude larger, and significantly offset from the previous ground-based measurements. Lower panel: Distance comparison for NGC 6397. We invert our parallax measurement to obtain a distance estimate (red); no upper error bar is shown as lower error bar on the parallax extended below zero, corresponding to unphysical results but effectively indicating that the upper limit on the distance uncertainty is infinite. We also show previous distance estimates from [Reid & Gizis \(1998\)](#) (orange, MS fitting), [Gratton et al. \(2003\)](#) (green, MS fitting), [Hansen et al. \(2007\)](#) (cyan, WD sequence), [Heyl et al. \(2012\)](#) (blue, dynamical), and the estimate from [Watkins et al. \(2015a\)](#) (purple, dynamical). Our distance uncertainties are significantly larger than previous estimates, however our distance estimate is consistent within the previous results within the very large error bars.

timed $D = 2.67^{+0.19}_{-0.18}$ kpc and [Gratton et al. \(2003\)](#) estimated $D = 2.54^{+0.10}_{-0.09}$ kpc, both via MS fitting; [Hansen et al. \(2007\)](#) measured $D = 2.54 \pm 0.07$ kpc by fitting the WD sequence; and [Heyl et al. \(2012\)](#) estimated $D = 2.2^{+0.5}_{-0.7}$ kpc and [Watkins et al. \(2015a\)](#) estimated $D = 2.39^{+0.13}_{-0.11}$ kpc by combining PMs and LOS velocities. We show these distance estimates along with our own in the lower panel of [Figure 7](#). Our result is larger than all of these previous estimates, but is consistent within 1σ .

3.5. NGC 6656 (M22)

For NGC 6656, we find parallax $\varpi = 0.509 \pm 0.222$ mas, RA PM $\mu_{\alpha^*} = 8.64 \pm 1.49$ mas/yr, and Dec PM $\mu_{\delta} = -5.09 \pm 1.45$ mas/yr, with correlation terms $\rho(\varpi, \mu_{\alpha^*}) = -0.194$, $\rho(\varpi, \mu_{\delta}) = -0.160$, and $\rho(\mu_{\alpha^*}, \mu_{\delta}) = 0.935$. In [Figure 8](#), the upper and middle panels show the parallaxes and PMs of the 2 TGAS stars (black) and our averages (red).

There are three previous PM estimates for NGC 6656: [Cudworth & Hanson \(1993\)](#) measured $\mu_{\alpha^*} = 8.6 \pm 1.3$ mas/yr and $\mu_{\delta} = -5.1 \pm 1.5$ mas/yr from the ground; [Chen et al. \(2004\)](#) measured $\mu_{\alpha^*} = 10.19 \pm 0.20$ mas/yr and $\mu_{\delta} = -3.34 \pm 0.10$ mas/yr using *HST*/WFPC2 data; and [CD13](#) measured

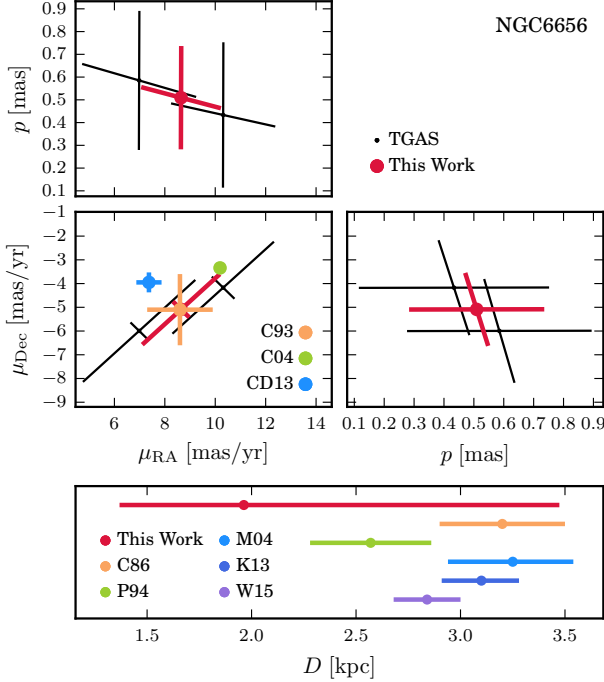


Figure 8. Upper and middle panels: Parallax and PM results for NGC 6656. The black points show the 2 TGAS stars we identified as cluster members. The red points shows the mean values we have calculated here. In the PM plot (middle left) we compare our estimate to values from Cudworth & Hanson (1993) (orange, ground-based), Chen et al. (2004) (green, *HST*), and CD13 (cyan, ground-based). The PMs we measure are consistent with the previous measurements, albeit with uncertainties an order of magnitude larger. Lower panel: Distance comparison for NGC 6656. We invert our parallax measurement to obtain a distance estimate (red). We also show previous distance estimates from Cudworth (1986) (orange, HB fitting), Peterson & Cudworth (1994) (green, dynamical), Monaco et al. (2004) (cyan, HB fitting), Kunder et al. (2013) (blue, RR Lyraes), and Watkins et al. (2015a) (purple, dynamical). Our distance uncertainties are significantly larger than previous estimates, however our distance estimate is consistent within the previous results within the our uncertainties.

$\mu_{\alpha*} = 7.37 \pm 0.50$ mas/yr and $\mu_{\delta} = -3.95 \pm 0.42$ mas/yr using a combination of photographic plates and ground-based CCD images. These points are shown in the PM panel (centre left) of Figure 8 as orange, green, and cyan points respectively. CD13 advises caution considering the Chen et al. (2004) *HST* result, as they note that bulge stars were used to create the reference frame and that possible (and likely) motion of the bulge stars was not factored into the analysis, nevertheless we do make a comparison here.

We find that our PM estimate is consistent with all three studies, indeed it is in exceptional agreement with the ground-based PM estimate from Cudworth & Hanson (1993). Contrary to the two previous clusters we do not find the best agreement with the previous *HST* estimate, possibly for the reasons discussed above.

Our parallax of $\varpi = 0.509 \pm 0.222$ mas corresponds to a distance of $D = 1.96^{+1.51}_{-0.59}$ kpc. There are a number of previous distance estimates in the literature obtained using different methods: Cudworth (1986) estimated $D = 3.2 \pm 0.3$ kpc (which is the value quoted in H96) and Monaco et al. (2004) estimated $D = 3.25^{+0.31}_{-0.29}$ kpc, both via HB fitting; Peterson & Cudworth (1994) measured $D = 2.57 \pm 0.29$ kpc and Watkins et al. (2015a) estimated $D = 2.84 \pm 0.16$ kpc by combining PMs and LOS velocities; and Kunder et al. (2013) estimated $D = 3.10^{+0.19}_{-0.18}$ kpc using RR Lyraes. We show these distance

estimates along with our own in the lower panel of Figure 8. This time, our result is lower than all of the previous estimates, but is consistent within the error bars. Once again, our distance uncertainties are an order of magnitude larger than for previous estimates.

4. ABSOLUTE SPACE MOTIONS

We can combine our PM estimates, with sky coordinates, distances and heliocentric radial velocities to determine the implied Galactocentric motion of the GCs. We use our PM estimates for this analysis, but not our distance (parallax) estimates, as it is clear those are not as accurate as literature values.

We adopt a Cartesian coordinate system (X, Y, Z) centred on the Galactic Centre, where the X -axis points in the direction from the Sun to the Galactic Centre, the Y -axis points in the direction of the Sun's Galactic rotation, and the Z -axis points towards the North Galactic Pole.

To transform the measured heliocentric velocities into velocities (U, V, W) in the Galactocentric rest frame, we adopt a distance from the Sun to the Galactic Centre of $R_0 = 8.29 \pm 0.16$ kpc, and a circular velocity of the local standard of rest (LSR) of $V_0 = 239 \pm 5$ km/s (both McMillan 2011). We also assume a solar peculiar velocity relative to the LSR of $(U_{\text{pec}}, V_{\text{pec}}, W_{\text{pec}}) = (11.10 \pm 1.23, 12.24 \pm 2.05, 7.25 \pm 0.63)$ km/s (Schönrich et al. 2010). To estimate Galactocentric velocities and their uncertainties, we use a Monte-Carlo scheme that propagates all observational distance and velocity uncertainties and their correlations, including those for the Sun. Our results are summarised in Table 4, but we discuss each cluster in turn below.

4.1. NGC 104

We adopt sky coordinates $(\alpha, \delta) = (6.024, -72.081)$ deg and heliocentric radial velocity $v_{\text{hel}} = -18.0 \pm 0.1$ km/s from H96, and distance $D = 4.61^{+0.20}_{-0.19}$ kpc from Bono et al. (2008). Then in the (X, Y, Z) coordinate system, the position vector of NGC 104 is $\mathbf{r} = (-6.38, -2.65, -3.25)$ kpc.

The Galactocentric velocity vector we determine is $\mathbf{v} = (-74.97 \pm 14.10, 145.23 \pm 13.12, 68.30 \pm 8.85)$ km/s, which gives a total velocity with respect to the MW of $v \equiv |\mathbf{v}| = 177.14 \pm 6.81$ km/s. The corresponding Galactocentric radial and tangential velocities are then $v_{\text{rad}} = -16.84 \pm 14.81$ km/s and $v_{\text{tan}} = 176.34 \pm 7.02$ km/s.

Zinn (1985) separated Galactic GCs into two subpopulations based on their metallicities and orbital properties: those belonging to the disk ($[\text{Fe}/\text{H}] > -0.8$) and those belonging to the halo ($[\text{Fe}/\text{H}] < -0.8$). Overall, the disk clusters have lower orbital eccentricity and are confined to the Galactic plane, while the halo clusters span a range of eccentricities and explore greater distances from the disk plane.

In their orbital analysis, Odenkirchen et al. (1997) noted that the orbital energy of NGC 104 is very close to its corresponding circular orbit (ie. the energy of a circular orbit at its current Galactocentric distance). They noted that the orbital properties of NGC 104 were somewhat offset from the rest of their sample, which were all thought to be halo clusters, and so concluded that NGC 104 is a disk cluster. This conclusion was also reached by Cudworth & Hanson (1993), who noted that the space velocity of NGC 104 marks it as a thick-disk cluster, despite its relatively large distance from the plane.

4.2. NGC 5272

Table 4
Cluster space motions and orbits.

Cluster	D	X	Y	Z	U	V	W	$ \mathbf{v} $	v_{rad}	v_{tan}
(1)	(kpc)	(kpc)	(kpc)	(kpc)	(km/s)	(km/s)	(km/s)	(km/s)	(km/s)	(km/s)
(1)	(2)	(3)	(4)	(5)	(6)	(7)	(8)	(9)	(10)	(11)
NGC 104	$4.61^{+0.20}_{-0.19}$	-6.38	-2.65	-3.25	-74.97 ± 14.10	145.23 ± 13.12	68.30 ± 8.85	177.14 ± 6.81	-16.84 ± 14.81	176.34 ± 7.02
NGC 5272	$10.05^{+0.97}_{-0.88}$	-6.83	1.32	9.86	49.87 ± 22.34	106.00 ± 23.90	-129.51 ± 4.83	174.63 ± 19.44	-122.42 ± 15.71	124.54 ± 23.87
NGC 6121	1.80 ± 0.05	-6.58	-0.27	0.50	55.10 ± 2.02	50.19 ± 8.42	2.13 ± 3.97	74.57 ± 6.38	-56.81 ± 2.35	48.30 ± 8.31
NGC 6397	$2.54^{+0.10}_{-0.09}$	-5.98	-0.92	-0.53	-61.20 ± 7.73	98.79 ± 16.28	-132.62 ± 14.60	176.34 ± 12.75	56.72 ± 10.39	166.97 ± 13.49
NGC 6656	$3.10^{+0.19}_{-0.18}$	-5.26	0.53	-0.41	-148.98 ± 4.97	212.58 ± 21.89	-119.23 ± 23.26	285.66 ± 21.25	178.12 ± 8.62	223.33 ± 21.22

Notes. Columns: (1) cluster name; (2) adopted distance (sources: [Bono et al. \(2008, NGC 104\)](#), [Ferraro et al. \(1999, NGC 5272\)](#), [Hendricks et al. \(2012, NGC 6121\)](#), [Gratton et al. \(2003, NGC 6397\)](#), and [Kunder et al. \(2013, NGC 6656\)](#)); (3) X position coordinate; (4) Y position coordinate; (5) Z position coordinate; (6) U velocity component; (7) V velocity component; (8) W velocity component; (9) magnitude of total velocity; (10) radial component of velocity; (11) tangential component of velocity.

We adopt sky coordinates $(\alpha, \delta) = (205.548, 28.377)$ deg and heliocentric radial velocity $v_{\text{hel}} = -147.6 \pm 0.2$ km/s from [H96](#), and distance $D = 10.05^{+0.97}_{-0.88}$ kpc from [Ferraro et al. \(1999\)](#). Then in the (X, Y, Z) coordinate system, the position vector of NGC 5272 is $\mathbf{r} = (-6.83, 1.32, 9.86)$ kpc.

The Galactocentric velocity vector we determine is $\mathbf{v} = (49.87 \pm 22.34, 106.00 \pm 23.90, -129.51 \pm 4.83)$ km/s, which gives a total velocity with respect to the MW of $v \equiv |\mathbf{v}| = 174.63 \pm 19.44$ km/s. The corresponding Galactocentric radial and tangential velocities are then $v_{\text{rad}} = -122.42 \pm 15.71$ km/s and $v_{\text{tan}} = 124.54 \pm 23.87$ km/s. NGC 5272 is currently located almost 10 kpc above the plane of the disk, so is extremely likely to be a halo cluster.

All five of the previous PM studies discussed in [Section 3.2](#) performed space motion analyses. [Cudworth & Hanson \(1993\)](#) found that the orbit of NGC 5272 was very uncertain in their analysis; nevertheless, they concluded that the orbit was more consistent with the [Zinn \(1985\)](#) halo population, as expected. Their space motion was somewhat different from the other studies, but all the other studies reached broadly similar conclusions: NGC 5272 is a halo cluster with a box-like orbit ([Scholz et al. 1993](#); [Wu et al. 2002](#)), and is likely near its apocentre ([Geffert 1998](#)).

4.3. NGC 6121

We adopt sky coordinates $(\alpha, \delta) = (245.897, -26.526)$ deg and heliocentric radial velocity $v_{\text{hel}} = 70.7 \pm 0.2$ km/s from [H96](#), and distance $D = 1.80 \pm 0.05$ kpc from [Hendricks et al. \(2012\)](#). Then in the (X, Y, Z) coordinate system, the position vector of NGC 6121 is $\mathbf{r} = (-6.58, -0.27, 0.50)$ kpc.

The Galactocentric velocity vector we determine is $\mathbf{v} = (55.10 \pm 2.02, 50.19 \pm 8.42, 2.13 \pm 3.97)$ km/s, which gives a total velocity with respect to the MW of $v \equiv |\mathbf{v}| = 74.57 \pm 6.38$ km/s. The corresponding Galactocentric radial and tangential velocities are then $v_{\text{rad}} = -56.81 \pm 2.35$ km/s and $v_{\text{tan}} = 48.30 \pm 8.31$ km/s. The proximity to the Galactic plane and the very small Z component of velocity imply that NGC 6121 spends most of its time in the disk.

Our space motion for NGC 6121 is in reasonable agreement with the analyses by [Dinescu et al. \(1999a\)](#) and [Bedin et al. \(2003\)](#), but shows best agreement with that calculated by [Kalirai et al. \(2004\)](#) – which is to be expected given the very good agreement between our PM determination and theirs – except for the sign of W . This sign discrepancy is not surprising as we find a very small W component that is consistent with both positive and negative W velocities within 1σ . Small changes in the assumed parameters will change whether the

sign of the W velocity, but this has little effect on our overall conclusions.

Both [Dinescu et al. \(1999a\)](#) and [Bedin et al. \(2003\)](#) found very radial orbits for NGC 6121, and their extreme eccentricities favour NGC 6121 as being a halo cluster on a very low inclination orbit and not a disk cluster. The PM determination of [Cudworth & Hanson \(1993\)](#) was significantly offset from all other previous estimates, however their conclusions on the orbit of NGC 6121 were nonetheless broadly similar.

[Dinescu et al. \(1999a\)](#) also estimated the tidal-shock rate of NGC 6121 based on its orbit and found that this is larger than the two-body relaxation time in the cluster; this indicates that tidal shocks due to the bulge and the disk have likely had a significant influence on the evolution of the cluster. Again it is not surprising that a cluster confined to the disk should be strongly affected by tides.

4.4. NGC 6397

We adopt sky coordinates $(\alpha, \delta) = (265.175, -53.674)$ deg and heliocentric radial velocity $v_{\text{hel}} = 18.8 \pm 0.1$ km/s from [H96](#), and distance $D = 2.54^{+0.10}_{-0.09}$ kpc from [Gratton et al. \(2003\)](#). Then in the (X, Y, Z) coordinate system, the position vector of NGC 6397 is $\mathbf{r} = (-5.98, -0.92, 0.53)$ kpc.

The Galactocentric velocity vector we determine is $\mathbf{v} = (-61.20 \pm 7.73, 98.79 \pm 16.28, -132.62 \pm 14.60)$ km/s, which gives a total velocity with respect to the MW of $v \equiv |\mathbf{v}| = 176.34 \pm 12.75$ km/s. The corresponding Galactocentric radial and tangential velocities are then $v_{\text{rad}} = 56.72 \pm 10.39$ km/s and $v_{\text{tan}} = 166.97 \pm 13.49$ km/s. NGC 6397 is also currently located close to the disk plane, however the high W velocity implies that it does move away from the plane and is most likely a halo cluster, as expected from its low $[\text{Fe}/\text{H}]$ metallicity.

This is consistent with more detailed orbital analyses by [Cudworth & Hanson \(1993\)](#) and [CD13](#) which concluded that NGC 6397 has a “typical halo-like orbit” (following [Zinn 1985](#)). [Milone et al. \(2006\)](#) found that NGC 6397 has a boxy orbit that oscillates rapidly through the disk. Thanks to the moderate eccentricity of the orbit, NGC 6397 does not move too far from the Galactic centre; thus, it passes through high-density regions of the disk and is expected to be affected by tidal shocks.

4.5. NGC 6656 (M 22)

We adopt sky coordinates $(\alpha, \delta) = (279.100, -23.905)$ deg and heliocentric radial velocity $v_{\text{hel}} = -146.3 \pm 0.2$ km/s from [H96](#), and distance $D = 3.10^{+0.19}_{-0.18}$ kpc from [Kunder et al. \(2013\)](#).

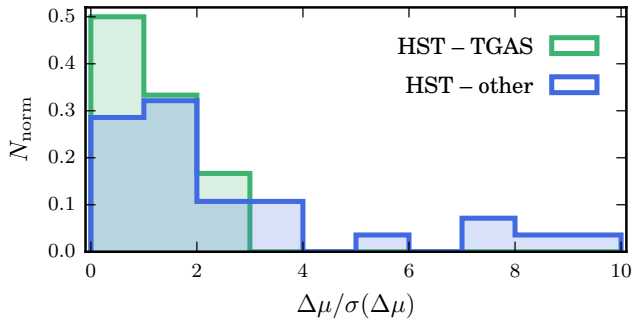


Figure 9. Normalised histograms of PM differences $\Delta\mu$ as a fraction of the uncertainty in the difference $\sigma(\Delta\mu)$ for all clusters, with RA PMs and Dec PMs considered independently. The blue histogram shows the offsets between *HST* PM measurements and other non-*HST* PM measurements, all taken from the literature (see Section 3). In some cases, the *HST* and non-*HST* measurements are discrepant at more than 5σ . The green histogram shows the offsets between literature *HST* PM measurements and our TGAS PM measurements. All *HST* and TGAS measurements agree within 3σ .

Then in the (X, Y, Z) coordinate system, the position vector of NGC 6656 is $\mathbf{r} = (-5.26, 0.53, -0.41)$ kpc.

The Galactocentric velocity vector we determine is $\mathbf{v} = (-148.98 \pm 4.97, 212.58 \pm 21.89, -119.23 \pm 23.26)$ km/s, which gives a total velocity with respect to the MW of $v \equiv |\mathbf{v}| = 285.66 \pm 21.25$ km/s. The corresponding Galactocentric radial and tangential velocities are then $v_{\text{rad}} = 178.12 \pm 8.62$ km/s and $v_{\text{tan}} = 223.33 \pm 21.22$ km/s. As for NGC 6397, NGC 6656 is currently located close to the disk plane but its W velocity suggests that it does move away from the disk, so it is more likely to be a halo cluster.

From detailed studies of the implied orbit, both Cudworth & Hanson (1993) and CD13 also conclude that NGC 6656 is a halo cluster. This is not surprising given that NGC 6656 is metal-poor and also shows signs of inhomogeneous element abundances (eg. Norris & Freeman 1983), which is thought to indicate extended star formation (eg. Marino et al. 2011) and point to an extragalactic origin (eg. Lee et al. 2009).

Similarly to NGC 6397, NGC 6656 is likely to be vulnerable to tides from repeated passages through the disk. This is borne out by observations: Ness et al. (2013) found a population of stars in their ARGOS study of the bulge that had properties consistent with NGC 6656, which could be extratidal stars from the cluster. Kunder et al. (2014) also found a candidate extratidal star of NGC 6656 in RAVE data.

5. CONCLUSIONS

We have identified a total of 20 members of 5 Galactic GCs in the TGAS catalogue from *Gaia* DR1 – 5 stars in NGC 104 (47 Tuc), 1 star in NGC 5272 (M3), 5 stars in NGC 6121 (M4), 7 stars in NGC 6397, and 2 stars in NGC 6656 – and used these stars to determine the PMs and parallaxes of these clusters. These first *Gaia* PMs for GCs provide new insights into their dynamics. The parallaxes instead, while consistent with existing knowledge, are not yet competitive with other methods for determining GC distances.

We reviewed all existing PM measurements for the GCs in our final sample. Existing PM estimates for the same cluster do not generally agree with each other within the random errors; in some cases, measurements disagree by 5σ or more (see Figure 9, blue histogram). Hence, the accuracy of the existing PM measurements is generally dominated by systematic errors, and not random errors, as is often the case in astrometry. By contrast, the TGAS catalogue combines mea-

surements from *Hipparcos* and *Gaia*: two space missions with stable and well-calibrated platforms designed specifically to do astrometry. The main value of our TGAS analysis is therefore that it provides a homogeneous study of multiple GCs based on an astrometric catalogue with well-controlled systematics.

We have not explicitly included possible *spatial* correlations in TGAS PM errors (Gaia Collaboration et al. 2016; Lindegren et al. 2016) in our analysis. The effect of such correlations would be to underestimate the random error in the weighted average PM of a stellar sample (Kroupa & Bastian 1997). *Gaia* DR1 has a nominal systematic positional accuracy of ~ 0.3 mas. Over the ~ 25 yr time baseline with the *Hipparcos* mission, this introduces a PM error of only ~ 0.01 mas/yr. van der Marel & Sahlmann (2016) found the agreement between TGAS and *HST* PMs for the Magellanic Clouds to be significantly better than $\lesssim 0.1$ mas/yr. This further bounds the size of any possible PM systematics. Systematic PM errors in the TGAS PMs are therefore well below the size of the random PM errors for our GCs in Table 3 (which range from 0.29–1.49 mas/yr).

The random PM errors from our analysis are comparable to those from many existing studies, but do not yet improve upon them. In general, the PM diagrams presented here show that our measurements are consistent with the “scatter clouds” of measurements from previous studies. Detailed assessment shows that our measurements are generally fully consistent with existing *HST*-based measurements (see Figure 9, green histogram), but not with all existing ground-based measurements. This agrees with the findings of van der Marel & Sahlmann (2016), who found excellent agreement between measurements of the PMs of the Magellanic Clouds from TGAS and *HST*. We therefore conclude that: (1) Since TGAS and *HST* use very different methods for astrometry, our GC results provide further external validation of both data sets and their underlying approaches; and (2) many ground-based GC PM measurements suffer from systematic uncertainties in excess of the random errors.

We also combined our PMs with literature radial velocities and distances to calculate absolute Galactocentric space motions for the clusters, corrected for peculiar motion of the Sun relative to the LSR and for rotation of the LSR about the Galactic Centre. Our space motions are broadly consistent with previous orbital analyses.

Our results highlight the promise of future *Gaia* data releases for the determination of parallaxes and PMs in Galactic GCs. Comparing parallax distances from *Gaia* with previous photometric and dynamical distance estimates will provide crucial verification of all three methods; and improved distances and PMs will further constrain GC orbits. With future releases, *Gaia* PMs will be able to resolve the internal motions of nearby Galactic GCs as well as measure global motions as we have done here.

Gaia PMs and *HST* PMs are highly complementary, as the two observatories have different strengths. At present, the majority of *HST* PMs for the inner GCs are relative, due to the difficulty of finding sufficient fixed background sources in the crowded GC fields that can be used to create an absolute reference frame (Bellini et al. 2014). This does not affect velocity dispersion or anisotropy determination (Watkins et al. 2015b) but does not allow for measurement of rotation, or indeed the global motion of the GC. *Gaia* PMs are absolute and so will provide crucial constraints on cluster rotation and on their global motions. By contrast, *HST* can measure PMs down

to fainter magnitudes, and so can go deeper for the nearby clusters, and can measure PMs for more distant clusters than *Gaia* will be able to achieve. Thus, *HST* PMs will be crucial for constraining the shape of the outer MW halo. *HST* will also provide more accurate astrometry in the crowded centres of clusters (though these regions are challenging even for *HST*).

For now, *HST* remains the best source of GC PMs, however, in the future the the best choice will depend on the particular science goals. Combined together, *Gaia* and *HST* PMs will provide the greatest coverage, depth and accuracy of all, and will revolutionise our understanding of both individual clusters and the entire MW GC population.

ACKNOWLEDGEMENTS

LLW wishes to thank Erik Tollerud for useful discussions. This research has made use of *Astropy*⁹, a community-developed core Python package for Astronomy (*Astropy Collaboration et al. 2013*). This research has made use of NASA's Astrophysics Data System. This work has made use of data from the European Space Agency (ESA) space mission *Gaia*¹⁰, processed by the *Gaia* Data Processing and Analysis Consortium (DPAC)¹¹. Funding for the DPAC has been provided by national institutions, in particular the institutions participating in the *Gaia* Multilateral Agreement.

REFERENCES

- Anderson, J., & King, I. R. 2003, *AJ*, 126, 772
 Astraatmadja, T. L., & Bailer-Jones, C. A. L. 2016, *ArXiv e-prints*, arXiv:1609.03424
 Astropy Collaboration, Robitaille, T. P., Tollerud, E. J., et al. 2013, *A&A*, 558, A33
 Bedin, L. R., Piotto, G., King, I. R., & Anderson, J. 2003, *AJ*, 126, 247
 Bellini, A., Anderson, J., van der Marel, R. P., et al. 2014, *ApJ*, 797, 115
 Bono, G., Stetson, P. B., Sanna, N., et al. 2008, *ApJ*, 686, L87
 Casetti-Dinescu, D. I., Girard, T. M., Herrera, D., et al. 2007, *AJ*, 134, 195
 Casetti-Dinescu, D. I., Girard, T. M., Jilková, L., et al. 2013, *AJ*, 146, 33
 Casetti-Dinescu, D. I., Girard, T. M., Korchagin, V. I., van Altena, W. F., & López, C. E. 2010, *AJ*, 140, 1282
 Chaboyer, B. 1995, *ApJ*, 444, L9
 Chen, D., Chen, L., & Wang, J.-J. 2004, *Chinese Physics Letters*, 21, 1673
 Cioni, M.-R. L., Bekki, K., Girardi, L., et al. 2016, *A&A*, 586, A77
 Cudworth, K. M. 1979, *AJ*, 84, 1312
 —. 1986, *AJ*, 92, 348
 Cudworth, K. M., & Hanson, R. B. 1993, *AJ*, 105, 168
 Cudworth, K. M., & Rees, R. 1990, *AJ*, 99, 1491
 Dinescu, D. I., Girard, T. M., & van Altena, W. F. 1999a, *AJ*, 117, 1792
 Dinescu, D. I., Girard, T. M., van Altena, W. F., & López, C. E. 2003, *AJ*, 125, 1373
 Dinescu, D. I., Girard, T. M., van Altena, W. F., Mendez, R. A., & Lopez, C. E. 1997, *AJ*, 114, 1014
 Dinescu, D. I., van Altena, W. F., Girard, T. M., & López, C. E. 1999b, *AJ*, 117, 277
 Dotter, A., Chaboyer, B., Jevremović, D., et al. 2008, *ApJS*, 178, 89
 Ferraro, F. R., Messineo, M., Fusi Pecci, F., et al. 1999, *AJ*, 118, 1738
 Freire, P. C., Camilo, F., Kramer, M., et al. 2003, *MNRAS*, 340, 1359
 Gaia Collaboration, Brown, A. G. A., Vallenari, A., et al. 2016, *ArXiv e-prints*, arXiv:1609.04172
 Geffert, M. 1998, *A&A*, 340, 305
 Gratton, R. G., Bragaglia, A., Carretta, E., et al. 2003, *A&A*, 408, 529
 Hansen, B. M. S., Anderson, J., Brewer, J., et al. 2007, *ApJ*, 671, 380
 Harris, W. E. 1996, *AJ*, 112, 1487
 Hendricks, B., Stetson, P. B., VandenBerg, D. A., & Dall'Orta, M. 2012, *AJ*, 144, 25
 Heyl, J. S., Richer, H., Anderson, J., et al. 2012, *ApJ*, 761, 51
 Høg, E., Fabricius, C., Makarov, V. V., et al. 2000, *A&A*, 355, L27
 Kalirai, J. S., Richer, H. B., Hansen, B. M., et al. 2004, *ApJ*, 601, 277
 Kalirai, J. S., Anderson, J., Richer, H. B., et al. 2007, *ApJ*, 657, L93
 Kallivayalil, N., van der Marel, R. P., & Alcock, C. 2006, *ApJ*, 652, 1213
 Kaluzny, J., Thompson, I. B., Rozyczka, M., et al. 2013, *AJ*, 145, 43
 Krauss, L. M., & Chaboyer, B. 2003, *Science*, 299, 65
 Kroupa, P., & Bastian, U. 1997, *New A*, 2, 77
 Kunder, A., Stetson, P. B., Cassisi, S., et al. 2013, *AJ*, 146, 119
 Kunder, A., Bono, G., Piffl, T., et al. 2014, *A&A*, 572, A30
 Kunder, A., Kordopatis, G., Steinmetz, M., et al. 2016, *ArXiv e-prints*, arXiv:1609.03210
 Küpper, A. H. W., Balbinot, E., Bonaca, A., et al. 2015, *ApJ*, 803, 80
 Lee, J.-W., Kang, Y.-W., Lee, J., & Lee, Y.-W. 2009, *Nature*, 462, 480
 Lindegren, L., Lammers, U., Bastian, U., et al. 2016, *ArXiv e-prints*, arXiv:1609.04303
 Mackey, A. D., & Gilmore, G. F. 2004, *MNRAS*, 355, 504
 Marconi, M., Caputo, F., Di Criscienzo, M., & Castellani, M. 2003, *ApJ*, 596, 299
 Marino, A. F., Sneden, C., Kraft, R. P., et al. 2011, *A&A*, 532, A8
 McLaughlin, D. E., & van der Marel, R. P. 2005, *ApJS*, 161, 304
 McMillan, P. J. 2011, *MNRAS*, 414, 2446
 Michalik, D., Lindegren, L., & Hobbs, D. 2015, *A&A*, 574, A115
 Milone, A. P., Villanova, S., Bedin, L. R., et al. 2006, *A&A*, 456, 517
 Monaco, L., Pancino, E., Ferraro, F. R., & Bellazzini, M. 2004, *MNRAS*, 349, 1278
 Neeley, J. R., Marengo, M., Bono, G., et al. 2015, *ApJ*, 808, 11
 Ness, M., Freeman, K., Athanassoula, E., et al. 2013, *MNRAS*, 432, 2092
 Norris, J., & Freeman, K. C. 1983, *ApJ*, 266, 130
 Odenkirchen, M., Brosche, P., Geffert, M., & Tucholke, H.-J. 1997, *New A*, 2, 477
 Paez, E., Martinez Roger, C., & Straniero, O. 1990, *A&AS*, 84, 481
 Pearson, S., Küpper, A. H. W., Johnston, K. V., & Price-Whelan, A. M. 2015, *ApJ*, 799, 28
 Peterson, R. C., & Cudworth, K. M. 1994, *ApJ*, 420, 612
 Peterson, R. C., Rees, R. F., & Cudworth, K. M. 1995, *ApJ*, 443, 124
 Reid, I. N., & Gizis, J. E. 1998, *AJ*, 116, 2929
 Robin, A. C., Reylé, C., Derrière, S., & Picaud, S. 2003, *A&A*, 409, 523
 Salaris, M., Held, E. V., Ortolani, S., Gullieuszik, M., & Momany, Y. 2007, *A&A*, 476, 243
 Sandage, A., & Cacciari, C. 1990, *ApJ*, 350, 645
 Scholz, R. D., Odenkirchen, M., & Irwin, M. J. 1993, *MNRAS*, 264, 579
 Schönrich, R., Binney, J., & Dehnen, W. 2010, *MNRAS*, 403, 1829
 Sirianni, M., Jee, M. J., Benítez, N., et al. 2005, *PASP*, 117, 1049
 Thompson, I. B., Kaluzny, J., Rucinski, S. M., et al. 2010, *AJ*, 139, 329
 van der Marel, R. P., & Sahlmann, J. 2016, *ArXiv e-prints*, arXiv:1609.04395
 Verde, L., Jimenez, R., & Feeney, S. 2013, *Physics of the Dark Universe*, 2, 65
 Watkins, L. L., van der Marel, R. P., Bellini, A., & Anderson, J. 2015a, *ApJ*, 812, 149
 —. 2015b, *ApJ*, 803, 29
 Webb, J. J., Leigh, N., Sills, A., Harris, W. E., & Hurley, J. R. 2014, *MNRAS*, 442, 1569
 Woodley, K. A., Goldsbury, R., Kalirai, J. S., et al. 2012, *AJ*, 143, 50
 Wu, Z.-Y., Wang, J.-J., & Chen, L. 2002, *Chinese J. Astron. Astrophys.*, 2, 216
 Zhu, L., Romanowsky, A. J., van de Ven, G., et al. 2016, *MNRAS*, 462, 4001
 Zinn, R. 1985, *ApJ*, 293, 424
 Zocchi, A., Gieles, M., Hénault-Brunet, V., & Varri, A. L. 2016, *MNRAS*, 462, 696

⁹ <http://www.astropy.org>

¹⁰ <http://www.cosmos.esa.int/gaia>

¹¹ <http://www.cosmos.esa.int/web/gaia/dpac/consortium>